Localized activation of the distant tail neutral line just prior to substorm onsets

Masakazu Watanabe,[1] Michael Pinnock,[2] Alan S. Rodger,[2] Natsuo Sato,[1]
Hisao Yamagishi,[1] A. Sessai Yukimatu,[1] Raymond A. Greenwald,[3]
Jean-Paul Villain,[4] and Marc R. Hairston[5]

Abstract. We have found flow burst features in the nightside ionosphere that are thought to be the ionospheric signature of distant tail reconnection. These are observed to form just prior to substorm onsets. Simultaneous observations by the Goose Bay-Stokkseyri dual HF radars and DMSP satellites provide the data. Our conclusions are based on equatorward flow bursts on the nightside during two isolated substorms that followed a long period of magnetospheric inactivity associated with a northward interplanetary magnetic field. Both flow bursts start ~60 min after the growth phase onset and last ~10–20 min until the expansion phase onset, migrating equatorward with time. Simultaneous DMSP observations of precipitating particles show that the flow burst occurs at the polar cap boundary, suggesting that the equatorward migration corresponds to the expansion of the polar cap during the growth phase. For one event, the reconnection electric field at 400 km altitude was 14 mV/m and its longitudinal scale was 290 km, which is equivalent to a reconnection voltage of 4.1 kV. For the other event, these values were 11 mV/m (reconnection electric field), 380 km (longitudinal scale), and 4.0 kV (reconnection voltage). In addition to the reconnection signatures, we discuss implications for substorm dynamics during the final stage of the substorm growth phase. The morphology indicates that the distant tail neutral line is activated ~1 hour after the growth phase onset and at the same time the nightside separatrix starts to move equatorward much faster than during the preceding early and middle growth phases. The 1-hour time lag would correspond to the timescale on which slow rarefaction waves from both northern and southern tail lobes converge in the equatorial magnetotail. The fast-moving separatrix on the nightside implies a rapid change of magnetotail configuration resulting from nonlinear enhancement and/or earthward movement of the cross-tail current for the last 10–20 min prior to the expansion phase onset.

1. Introduction

Magnetic reconnection is one of the fundamental physical processes of magnetospheric physics; many magnetospheric phenomena are well organized by the magnetic reconnection scenario. Its most noticeable success is an explanation of convective flows within the magnetosphere. Large-scale convection patterns resulting from reconnection between the interplanetary and geomagnetic fields have been established as a paradigm of magnetospheric phenomenology. For periods of southward interplanetary magnetic field (IMF), reconnection on the dayside magnetopause couples the solar wind electric field with the terrestrial magnetosphere, and this coupling transfers open magnetic flux to the magnetotail. Subsequent reconnection in the magnetotail transfers closed magnetic flux to the dayside. The evidence for these processes comes from the strong dependence of the polar cap potential on the solar wind electric field [*Reiff et al.*, 1981] and the IMF control of ionospheric convection patterns [e.g., *Heelis*, 1984]. In these processes, solar wind energy is transported first into the magnetotail and then to the inner magnetosphere. The solar wind energy brought into the magnetosphere in this way produces a wide range of magnetospheric phenomena associated with storms and substorms, such as particle injection and energization at geosynchronous altitude, auroral particle precipitation into the atmosphere, and enhancement of field-aligned and ionospheric currents. Thus magnetic reconnection plays an important role in the energetics of the magnetosphere.

Plasma convection in the polar ionosphere is a necessary corollary of magnetospheric processes. Recently, several attempts have been being made to measure and monitor magnetic reconnection using ionospheric radar techniques (see the review of reconnection measurements below). The main purpose of this paper is to describe a newly found signature of nightside reconnection processes as observed by ionospheric radars. In the ionosphere, the consequence of magnetic reconnection is expected to appear as bursts or enhancements of plasma flow [*Cowley and Lockwood*, 1992]. Although there have been many reports of ionospheric signatures of dayside reconnection, little is known about nightside reconnection. In

[1]National Institute of Polar Research, Tokyo, Japan.
[2]British Antarctic Survey, Natural Environment Research Council, High Cross, Cambridge, England.
[3]Applied Physics Laboratory, Johns Hopkins University, Laurel, Maryland.
[4]Laboratoire de Physique et Chimie de l'Environnement, Centre National de la Recherche Scientifique, Orléans, France.
[5]William B. Hanson Center for Space Sciences, University of Texas at Dallas, Richardson, Texas.

this study, we have found mesoscale bursts of flow that are relevant to distant tail reconnection. Section 2 will be devoted to the demonstration of this phenomenon.

In addition to the reconnection signatures themselves, the flow burst phenomenon is very interesting in that it occurs at the end of the substorm growth phase just prior to the expansion phase onset. A secondary purpose of this paper is to discuss implications for substorm dynamics from the morphology of the flow bursts. Since magnetic reconnection is a boundary layer process, we need to trace the location of this boundary in the ionosphere. As a by-product, we can learn the time variation of the boundary, and consequently, of the magnetospheric configuration. Magnetospheric substorms have undergone 30 years of study. Although some aspects of their morphology are fairly well understood, others are still controversial and the basic physics remains unknown. We think our present results can contribute significantly to efforts to model substorms. In section 3.4, we will discuss the manifestations of the substorm morphology revealed by this study.

Before we present the data, it is useful to review past research on ionospheric measurements of magnetic reconnection. The theoretical background for reconnection measurements in the ionosphere was given by *Vasyliunas* [1984] and developed by *de la Beaujardière et al.* [1991] (see also *Blanchard et al.* [1996]). Energy, mass, and momentum flow across the open-closed boundary (which is referred to as the separatrix) is controlled by the electric field imposed on the X line. The electric field on the X line is called the reconnection electric field or reconnection rate. Under the assumption of frozen-in magnetic field lines, the reconnection electric field (E_{rec}) maps into the ionosphere along the field lines of the separatrix and can be measured in the ionosphere. The rate at which magnetic flux is transported across the separatrix with length dl is given by

$$E_{rec} \cdot d\mathbf{l}_{X\,line} = [\mathbf{B} \times (\mathbf{V} - \mathbf{U}) \cdot d\mathbf{l}]_{ionosphere}$$

where **B** represents the magnetic field, and **V** and **U** denote the plasma and separatrix velocities in the frame of reference. The voltage integrated along the X line is called the reconnection voltage.

As noted above, in order to show the presence of reconnection, it is necessary to determine the relative velocity between plasma flow and the separatrix motion. Using incoherent scatter radar data obtained at Sondrestromfjord, *de la Beaujardière et al.* [1987] showed, in an example from the 1400–1600 MLT (magnetic local time) region, that the ionospheric flow was poleward during the time of polar cap expansion. In their study, the convection reversal boundary was taken to be the polar cap boundary. Using the same facility, *de la Beaujardière et al.* [1991] estimated the reconnection rate (electric field) on the nightside; that was the first quantitative study of reconnection measurements. *Blanchard et al.* [1996] refined *de la Beaujardière et al.*'s [1991] work and investigated the dependence of the nightside reconnection rate on MLT, interplanetary physical parameters, and substorm activities. Using Goose Bay HF-radar data, *Baker et al.* [1997] measured the dayside reconnection rate during a Geospace Environment Modeling (GEM) campaign period.

In all these previous studies, the main difficulty was to determine the location of the separatrix, and this was the prime source of errors. In the postnoon observations by *de la Beaujardière et al.* [1987], the east-west reversal of large-scale convection was taken as the location of the separatrix. The justi-fication for this interpretation was that the poleward edge of electron precipitation observed by the NOAA 7 satellite was very near to the convection reversal. However, the convection reversal does not necessarily coincide with the polar cap boundary. *Lockwood et al.* [1989] used EISCAT radar observations in the 0300–0700 MLT sector to show that the poleward convection velocities at the convection reversal boundary consistently exceeded the poleward motion of the boundary when both plasma flow and convection reversal motion were poleward. They interpreted this to mean that the convection reversal lay some distance equatorward of the open-closed field line boundary. In the nightside work of *de la Beaujardière et al.* [1991], a sharp cutoff in the electron density in the E region was assumed to correspond to the sharp cutoff of precipitating electrons at the polar cap boundary. In addition to the E region electron density, *Blanchard et al.* [1996] used observations of 630-nm auroral emissions as a diagnostic tool of the polar cap boundary as suggested by *Blanchard et al.* [1995, 1997]. In the dayside work of *Baker et al.* [1997], line-of-sight Doppler spectral widths were used as a key parameter to identify the dayside cusp. This choice was based on a previous interpretation of broad spectral widths as the ionospheric signature of the cusp in HF radar data [*Baker et al.*, 1990, 1995]. Thus the determination of the open-closed boundary location is crucial for proper reconnection studies.

In this paper, we presume that the migration of the flow burst region is the motion of the polar cap boundary itself. This assumption is supported by the simultaneous particle observations with the DMSP satellites. We also show that in certain cases backscattered power peaks can be used as a tracer of the reconnection region.

2. Observations

From the survey of Super Dual Auroral Radar Network (SuperDARN) data in October and November 1995, we have found four similar flow burst events in the nightside ionosphere that occurred during the growth phase of an isolated substorm. In two events of the four, simultaneous observations of DMSP satellites in the radar field of view enabled us to reveal the physics of the flow burst. In this paper, we report these two flow burst events observed by the Goose Bay-Stokkseyri dual HF radars: one on November 16, 1995, and the other on October 27, 1995. Both occurred just prior to the substorm expansion phase onset and showed nearly the same features. We think the two events are essentially the same.

The Goose Bay and Stokkseyri radars are a pair of radars forming part of the SuperDARN designed to image global ionospheric convection over large spatial regions. The SuperDARN radars operate at frequencies between 8 and 20 MHz and measure the coherent backscattered power and Doppler spectral characteristics of decameter-range field-aligned irregularities in the E and F regions. At F region altitudes, the line-of-sight Doppler velocity of the irregularities gives a measure of the electric field drift of the plasma. Normally, the SuperDARN radars scan over an azimuthal sector in 16 beam steps every two minutes, and the backscatter returns are range-gated in steps of 45 km. The SuperDARN radars are located in pairs in order to measure a common volume by two radars. In the common viewing area of each radar pair, a two-dimensional map of plasma convection is produced every 2 min by combining the line-of-sight Doppler velocities from both

Table 1. Locations of HF Radars and Geomagnetic Observatories

	Geographic Latitude, °N	Geographic Longitude, °E	Geomagnetic (AACGM) Latitude, °N	Geomagnetic (AACGM) Longitude, °E
Goose Bay radar (Canada)	53.3	−60.5	61.7	23.2
Stokkseyri radar (Iceland)	63.9	−22.0	64.9	67.4
Dawson (Canada)	64.1	−139.1	66.1	−88.7
Meanook (Canada)	54.6	−113.3	62.2	−55.0
Fort Churchill (Canada)	58.8	−94.1	69.3	−28.7
Ottawa (Canada)	44.4	−75.5	55.3	0.7
Thule (Greenland)	77.5	−69.2	85.7	33.6
Narssarssuaq (Greenland)	61.2	−45.4	66.5	44.0
Tromsø (Norway)	69.7	18.9	66.5	103.5

radars. For a detailed description of the SuperDARN project, see *Greenwald et al.* [1995, and references therein].

During the time intervals of the two events analyzed here, the SuperDARN radars operated in the normal mode. The Goose Bay and Stokkseyri radars observe a large volume of the ionosphere above northeastern Canada and Greenland. The locations of the radars are listed in Table 1. In this paper, we show exclusively the Goose Bay data, although the vector determinations involve implicit use of Stokkseyri data. The Goose Bay radar scans over a 52° azimuth sector centered on 5° east of geographic north. Plates 1 and 3 show examples of backscatter echoes obtained with the Goose Bay radar and are plotted in the AACGM (altitude adjusted corrected geomagnetic) coordinate system based on the International Geomagnetic Reference Field Epoch 1995. In this paper, we assume that all the F region echoes are scattered from an altitude of 400 km. For a practical algorithm for computing the AACGM coordinate system, see *Bhavnani and Hein* [1994, and references therein]. Throughout this paper, magnetic latitude (MLAT) and magnetic longitude (MLON) are expressed in the AACGM coordinate system.

As mentioned in the introduction, determining the separatrix location is crucial to the reconnection measurements. For this purpose, we used DMSP F10 and DMSP F12 particle data. We also used the ion drift meter data on board DMSP F12 to complement the particle data. Both satellites carried electrostatic analyzers (SSJ/4) designed to measure the flux of precipitating electrons and ions in the energy range from 30 eV to 30 keV in 19 logarithmically spaced steps. For details of the SSJ/4 instrument, see *Hardy et al.* [1984]. The ion drift meter on DMSP F12 is part of the thermal plasma detector array called Special Sensor for Ions, Electrons, and Scintillation (SS-IES) and measures angles of ion arrival. The measured angles are converted into the two ion drift components perpendicular to the spacecraft's velocity vector. For details about the SSIES instrumentation, see *Greenspan et al.* [1986].

2.1. November 16, 1995, Event

The first event occurred on November 16, 1995. Figure 1 shows the horizontal component (positive geomagnetic north) of ground-based magnetic records obtained at Thule (THL, near geomagnetic north pole), Fort Churchill (FCC, auroral zone in the evening sector), Ottawa (OTT, midlatitude in the evening sector), Narssarssuaq (NAQ, premidnight auroral zone), and Tromsø (TRO, midnight auroral zone). The location of each magnetic observatory is listed in Table 1. Prior to 2219 UT on November 16 (the vertical dashed line on the left),

the magnetograms do not show any significant disturbance, indicating that the magnetosphere was quiet. At 2219 UT, an eastward electrojet started to grow in the evening sector as indicated by the positive excursions at Fort Churchill and Ottawa. At this time, positive magnetic deflections were also observed at Thule and Narssarssuaq. These observations suggest that the growth phase of a substorm started at 2219 UT. At 2327 UT, a sharp negative bay started at Tromsø as denoted by the vertical dashed line on the right, which is the onset of the substorm expansion phase. Magnetic field data obtained by IMP 8 indicated that the near-Earth IMF was persistently northward ($B_z \approx 1$–5 nT, in geocentric solar magnetospheric (GSM) coordinates) for ~8 hours before the start of the substorm growth phase, except for the two weak ($B_z \approx -1$ nT) southward excursions at 1845 and 2005 UT and the data dropout after 2043 UT. Thus the substorm followed a long period of a quiet magnetosphere ($K_p = 0_+$ or 1_-) associated with a northward IMF. The time interval bounded by the two vertical dashed lines is the growth phase of the substorm. The bursty flow we describe below occurred from 2316 to 2332 UT as designated by the horizontal bar in the bottom panel of Figure 1 (Tromsø magnetogram), most of which corresponded to the late growth phase just prior to the expansion phase onset.

Plate 1 shows a time sequence of Doppler velocities observed by the Goose Bay radar for each 2-min scan from 2310 to 2334 UT. The center of the field of view is in the 2000–2100 MLT sector. Blue represents velocities toward the radar (positive values), whereas red shows velocities away from the radar (negative values). In Plate 1e (2318–2320), we can see a localized light-blue region of enhanced equatorward bursty flow in the middle of the field of view (indicated by a yellow arrow). Doppler velocities of this region are greater than 750 m/s toward the radar. This flow burst is the subject of our present study. In the next scan (Plate 1f, 2320–2322), the bursty flow is also discernible as a light-blue (>750 m/s) region, but its location has migrated a little equatorward as compared with the previous scan. In the next two scans (Plates 1g and 1h, 2322–2326), the bursty flow region continues to exist, well isolated by its surrounding regions, and its location migrates further equatorward with time. At the next scan (Plate 1i, 2326–2328) when the expansion phase onset occurred, the major bursty flow has almost disappeared, although a light-blue high flow speed region can be identified as indicated by the yellow arrow. This high flow speed region can be traced in the next two scans (Plates 1j and 1k, 2328–2332), but it finally dies away at ≈2332 (Plate 1l, 2332–2334). To return to the start of the bursty flow, the equatorward migrating flow burst can be traceable up to
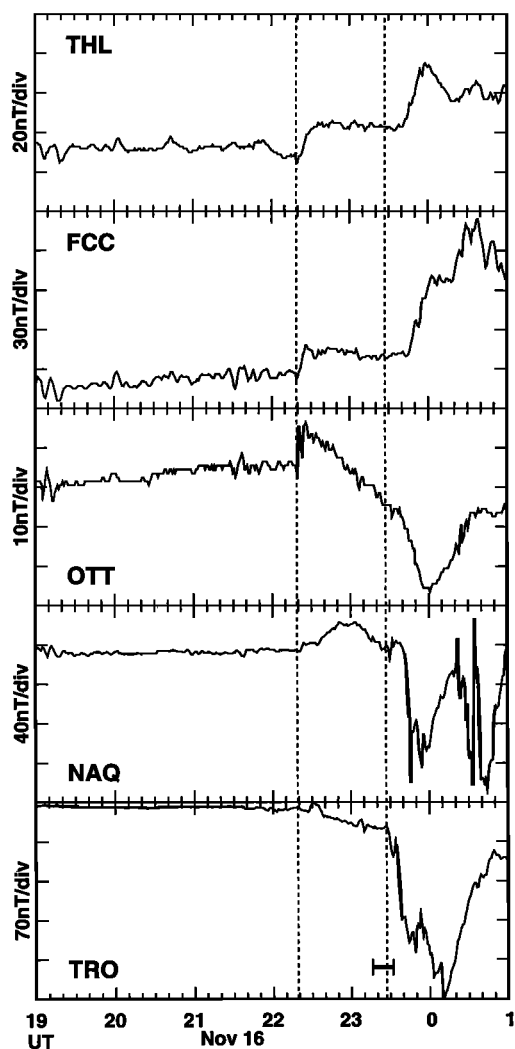
Figure 1. The horizontal component (positive geomagnetic north) of the geomagnetic field observed on November 16, 1995, at Thule (THL), Fort Churchill (FCC), Ottawa (OTT), Narssarssuaq (NAQ), and Tromsø (TRO) (see Table 1). The vertical dashed lines show the start of the substorm growth phase (2219 UT) and the onset of the expansion phase at Tromsø (2327 UT). The bursty flow occurred during the time interval designated by the horizontal bar in the bottom Tromsø magnetogram.

the scan of Plate 1d (2316–2318), although its main part is somewhat contaminated by noise. However, we cannot trace the bursty flow prior to that scan; in the preceding three scans (Plates 1a–1c), we cannot discern a significant high flow speed region. To sum up, an equatorward bursty flow region with velocities greater than 750 m/s emerged abruptly at ≈ 2316 (Plate 1d) and migrated equatorward with time; it started to degenerate at the substorm expansion phase onset (≈ 2326, Plate 1i) and finally faded out at ≈ 2332 (Plate 1l).

Plasma velocities shown in Plate 1 are only the line-of-sight component observed by the Goose Bay radar. The Stokkseyri radar, located to the east of the Goose Bay radar (see Table 1), was also operational and enabled the production of two-dimensional maps of plasma convection in the common viewing area of the two radars. Figure 2 shows these maps during the interval of major flow bursts (2318–2326 UT). A velocity

map is produced for each 2-min scan; Figures 2a–2d correspond, respectively, to Plates 1e–1h. The tail end of each arrow is the point where the vector is determined. In order to obtain overall smooth convective flow, we have used a median filter and a divergence-free relaxation technique in composing the Doppler velocities (therefore the line-of-sight component of vector velocities seen from Goose Bay in Figure 2 does not necessarily coincide with the Doppler velocities presented in Plate 1).

To quantify the accuracy of the vectors in Figure 2, we made histograms of errors in the total magnitude and of errors in one component (north-south or east-west) of the calculated vectors. The mode of the total magnitude error was 110 m/s, and its upper quartile (ninth decile) was 139 m/s (195 m/s). Similarly, the mode of the one-component error was 50 m/s, and its upper quartile (ninth decile) was 94 m/s (144 m/s). These indicate that the uncertainty of the vectors in Figure 2 is typically 100 m/s and mostly <200 m/s. In Figure 2, vectors with magnitude <100 m/s are replaced with solid circles.

The shaded areas in Figure 2 are the high flow speed (> 750 m/s) regions which appeared in Plate 1. Velocity vectors in these bursty flow regions are directed almost toward the Goose Bay radar site. Therefore we can discuss the flow burst characteristics using exclusively Goose Bay line-of-sight velocity data.

During the time interval of the bursty flow, DMSP F12 passed over the field of view of the Goose Bay radar flying poleward at an altitude of ~840 km. Plate 2 shows energy versus time spectrograms of precipitating electrons (middle) and ions (bottom) in the energy range from 30 eV to 30 keV. Note for ions the energy range is inverted, i.e., energy increasing downward. The transition from plasma sheet to polar cap is a little vague in this case. However, we can discern in the electron spectrogram that the envelope of the cutoff-energy in the energy flux breaks off at 2324:34 UT (69.5°N, 42.5°E in AACGM coordinates) as designated by the yellow wedge. After that time, the electron precipitation pattern shows a polar-rain-like signature. As for ion precipitation, the energy flux drops off a little equatorward of that point. Although there is a detached region of ions with energies of ≈ 200 eV poleward of that point, we infer that 2324:34 UT is the polar cap boundary, namely, the open-closed boundary. A possible interpretation of the detached region of ions will be explored in section 3.1.3.

The trajectory of DMSP F12 is shown in Plate 1h by an orange curve. The polar cap boundary is observed within this scan. The blue triangle on the trajectory shows the polar cap or open-closed (O/C) boundary observed at 2324:34 UT. The satellite trajectory is also plotted in Figure 2d, with the solid triangle on the trajectory denoting the open-closed (O/C) boundary. We can conclude from Plate 1h and Figure 2d that the flow burst occurred at or a little equatorward of the polar cap boundary, showing that the bursts of flow are consequences of a boundary layer process. (It will prove to be reconnection.) Although this picture is only a snapshot at one scan for 2324–2326 UT, it is reasonable to conclude that the equatorward migration of the bursty flow region corresponds to the equatorward motion of the polar cap boundary during the late substorm growth phase just prior to the expansion phase onset.

The top panel in Plate 2 shows the horizontal cross-track ion drift (positive westward) observed by the ion drift meter during the time interval given by the spectrograms. In the equatorward part of the plasma sheet, the ion drift is westward show-
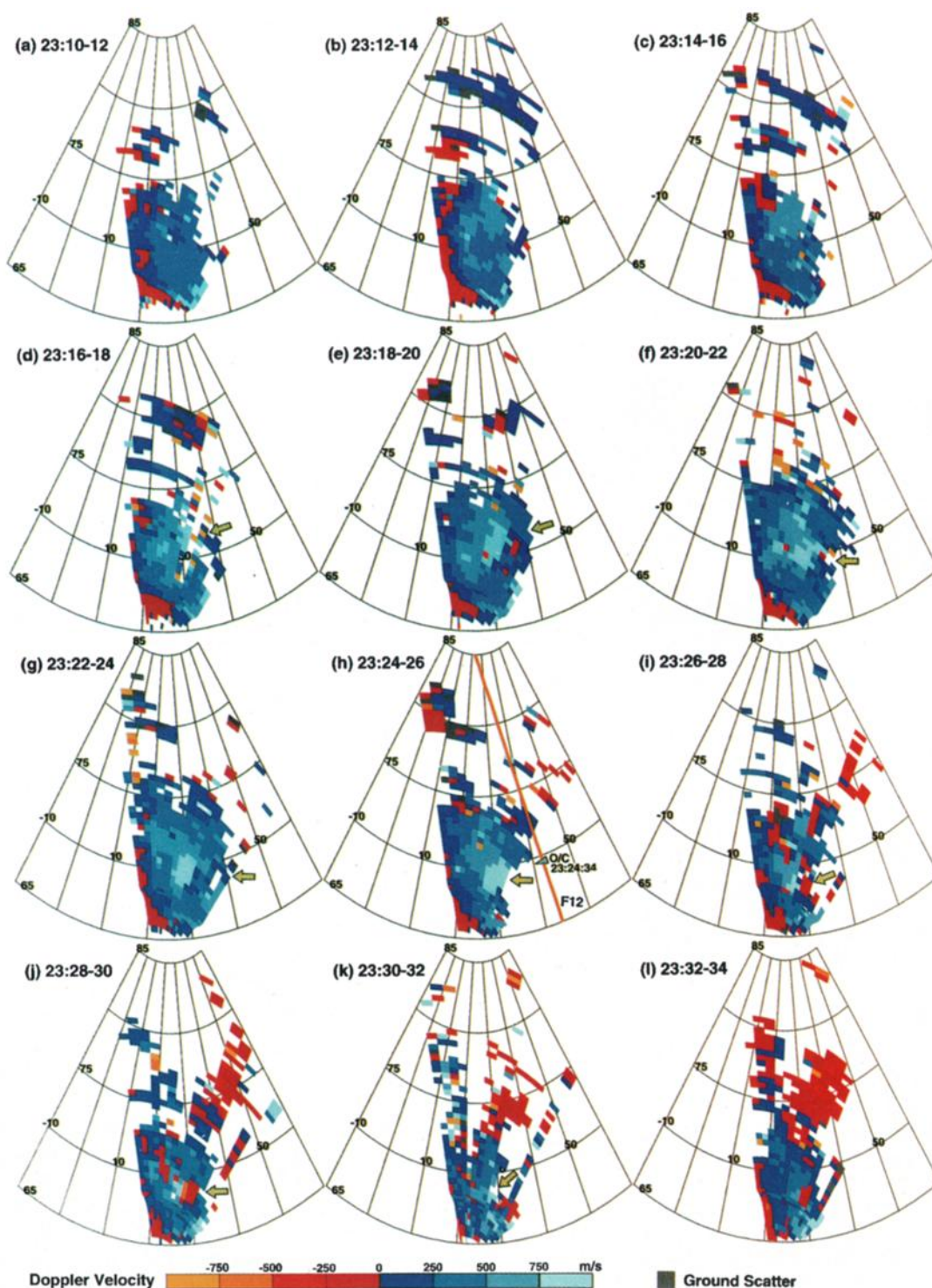
Plate 1. A time sequence of line-of-sight Doppler velocities observed by the Goose Bay radar during 2310–2334 UT on November 16, 1995. Two-dimensional maps were obtained every 2 min. Blue represents velocities toward the radar (positive values), whereas red shows velocities away from the radar (negative values). The bursts of flow, designated by yellow arrows, emerged at ≈ 2316 UT (Plate 1d) and started to degenerate at ≈ 2326 UT (at the onset of the substorm expansion phase, Plate 1i), and finally faded out at ≈ 2332 UT (Plate 1l). DMSP F12 passed over the field of view during this interval and observed the polar cap or open-closed (O/C) boundary at 2324:34 UT (69.5°N, 42.5°E in AACGM coordinates). The trajectory of the satellite is shown in Plate 1h by an orange curve with the blue triangle marking the open-closed boundary.
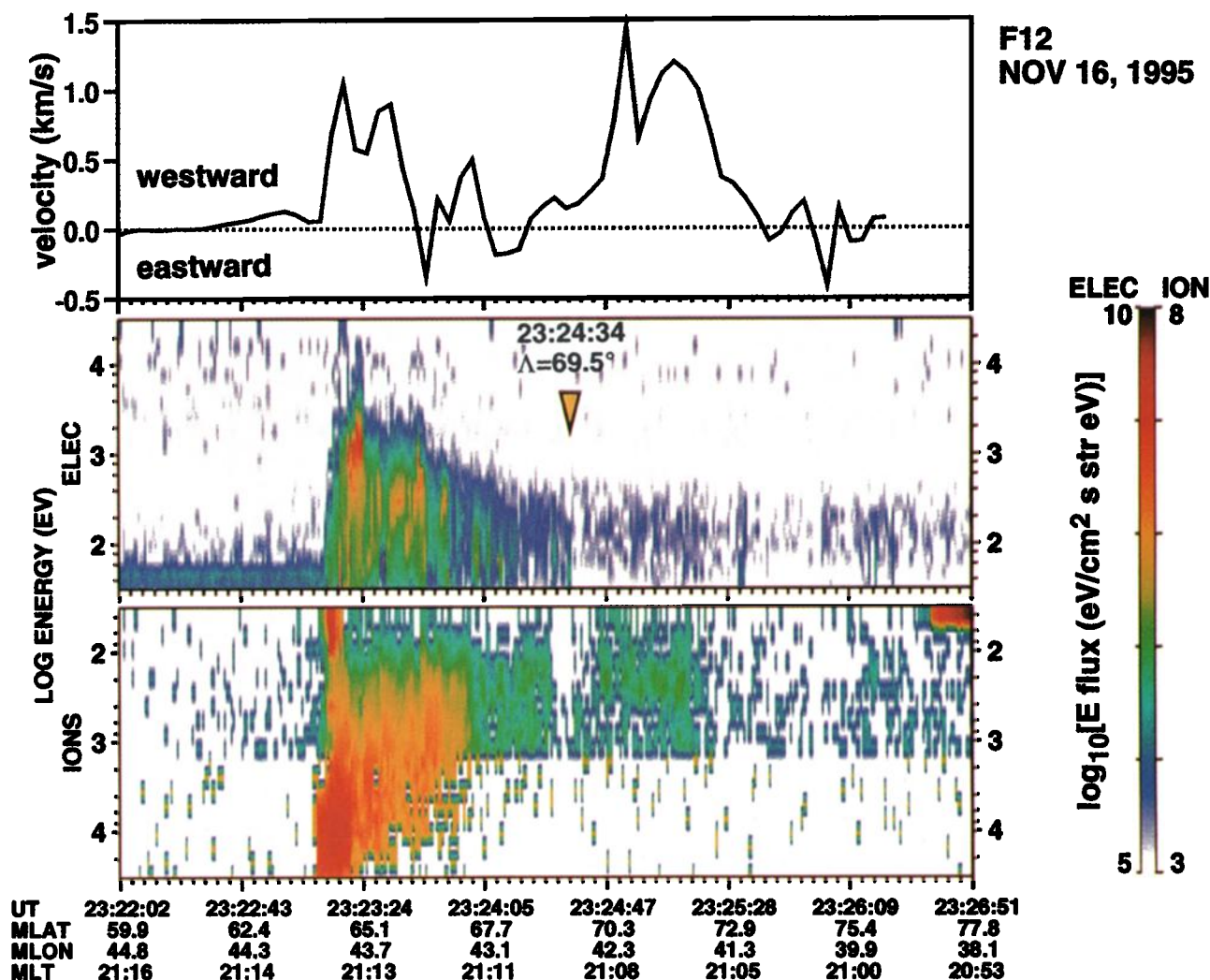
Plate 2. (middle and bottom) Energy versus time spectrograms of precipitating electrons (middle, energy increasing upward) and ions (bottom, energy increasing downward) observed by the DMSP F12 satellite for the November 16, 1995, event. The yellow wedge in the middle panel designates the transition from plasma-sheet-like to polar-rain-like electron precipitation, which we infer is the open-closed boundary. The time and magnetic latitude of the open-closed boundary observation are shown in the middle panel. (top) Horizontal ion drift velocities (cross-track component) observed simultaneously by the DMSP F12 satellite.

ing that the satellite was in the eveningside convection cell. In the poleward part of the plasma sheet, the ion drift oscillates between westward and eastward flows and exhibits no systematic flow direction until the open-closed boundary. At the open-closed boundary (69.5° MLAT), the drift velocity starts to rise steeply and reaches two peaks (1444 m/s at 70.8° MLAT and 1197 m/s at 71.2° MLAT). Then it decreases down to nearly zero at 73.6° MLAT, and after that it shows irregular variation. Thus, just poleward of the inferred open-closed boundary, there is a region of strong westward flows with 1000 m/s or more. Note that this westward flow region is associated with the detached ions we noted previously. A possible interpretation of this westward flow will be given in section 3.1.2.

The ion drift meter observation is consistent with the HF radar observation. Figure 2d shows that a westward flow region just poleward of the open-closed boundary was observed within this scan. Although the satellite traversed the eastern edge of the two-dimensional vector map, we can compare the radar and satellite observations. Plasma flows in the satellite

track meridian observed by the radars are directed westward at latitudes higher than the open-closed boundary. There are three vectors along the satellite track from 71.9° to 73.4° MLAT that nearly overlap the satellite observation. The absolute values of the three vectors are, from equatorward to poleward, 633, 508, and 399 m/s. The satellite observations that are nearest to these three vectors are 1129, 712, and 220 m/s, respectively. Since the calibration factor between the satellite altitude (840 km) and the radar scatter altitude (assumed to be 400 km) is nearly unity (the radar observations should be ~90% of the satellite observations), these values are qualitatively in agreement, at least in the decreasing trend with increasing latitude. However, the two observations do not necessarily show quantitative agreement.

We considered possible causes of the large discrepancy between the DMSP and radar observations. The radar measurements of the westward plasma flow are mainly contributed by the Stokkseyri line-of-sight velocity data. Uncertainties in the radar observation come from (1) errors in line-of-sight veloc-
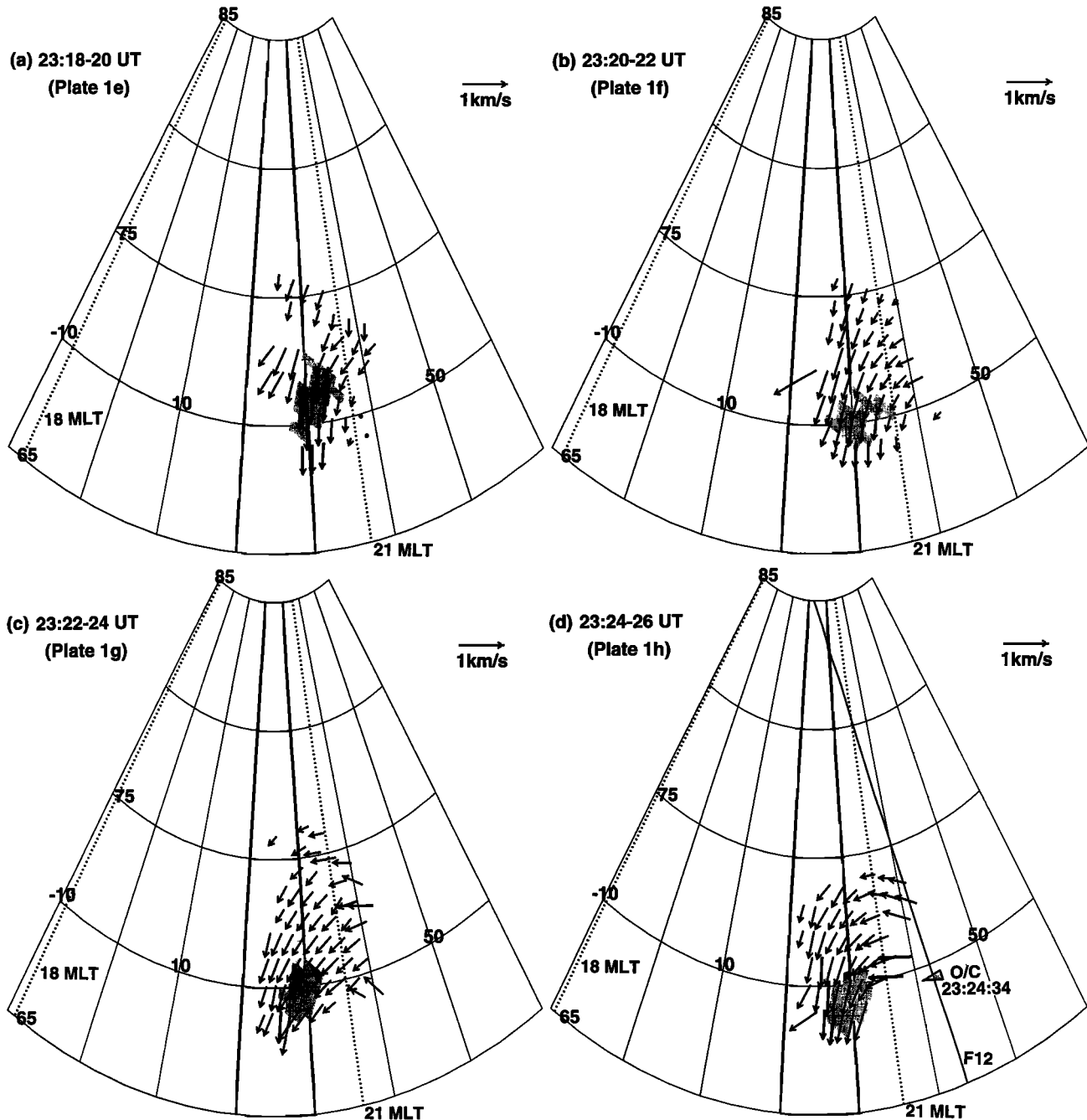
Figure 2. Two-dimensional velocity vectors during four scans between 2318 and 2326 UT on November 16, 1995, determined by combining the line-of-sight components from both Goose Bay and Stokkseyri data. Figures 2a–2d correspond, respectively, to Plates 1e–1h. The tail end of each arrow represents the point of observation. Vectors with magnitude less than 100 m/s are replaced with solid circles. The gray shaded areas show the flow burst region associated with >750 m/s velocities (light-blue regions in Plate 1). A median filter technique and divergence-free relaxation are used for smoothing the vectors. The solid curve in Figure 2d represents the trajectory of DMSP F12, and the filled triangle on the curve denotes the open-closed (O/C) boundary observation at 2324:34 UT.

ity, (2) broad spectral width, and (3) averaging a large volume to produce the line-of-sight velocity used in the vector calculation. We checked the three possibilities above and found that the broad spectral width is contributing most to the uncertainties in this case. The average spectral widths of the three points observed by the Stokkseyri radar are, from equatorward to poleward, 303, 361, and 359 m/s. Thus the values are quite

large. This suggests that the flows are quite turbulent within the radar sampling cell. The radar line-of-sight velocity is derived from the scatter that gives the largest power. The satellite may be seeing another component within the sampling cell that does not return the largest radar backscattered power.

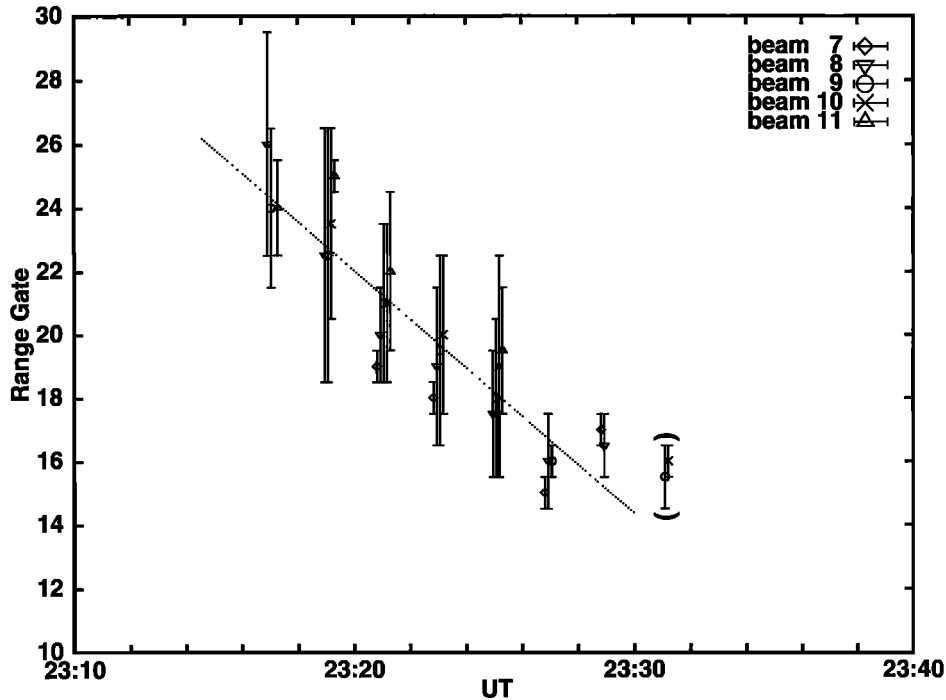Now we return to the flow burst. We have shown that the

Figure 3. The range gate extent of the "flow burst region" on November 16, 1995, defined as the region of equatorward velocities greater than 750 m/s (Plates 1d–1k). One range gate corresponds to 45 km. Beam numbers are labeled in order of number from the westernmost beam (beam 0) to the easternmost beam (beam 15). The data in parentheses are excluded from the analysis because of high error values. The oblique dotted line shows the linear regression fit. The boundary motion speed determined from the linear regression is 575±42 m/s.

bursty flow occurs at the polar cap boundary, suggesting that the equatorward migration of the bursty flow region is a manifestation of equatorward motion of the separatrix. With this assumption, we can determine the velocity of the separatrix. Figure 3 shows the range (latitudinal) width of the "flow burst region" which appeared in Plate 1. Here we define the flow burst region as a region with equatorward velocities >750 m/s. The criterion of 750 m/s will be justified below by the resultant boundary motion speed (i.e., separatrix motion speed) determined from this criterion. Beam numbers are labeled in order of number from the westernmost beam (beam 0) to the easternmost beam (beam 15). On average, the flow burst region was centered on beam 9. For the last scan during the bursty flow interval (scan for 2330–2332, Plate 1k), error estimates of Doppler velocities for all the range-beam bins of the flow burst region were >150 m/s. As explicitly shown below, we have used a criterion of 150 m/s for a maximum error value for the data to be effective in calculating mean values of Doppler velocities in the flow burst region. Hence, in Figure 3, the flow burst region in the last scan is put in parentheses. The oblique dotted line in Figure 3 is a linear regression line of the boundary motion; the last-scan data in parentheses are not included in the regression. Here one range gate corresponds to 45 km. Therefore, from the linear regression analysis, the speed of the boundary motion is estimated to be 575±42 m/s. The difference between the criterion speed for the identification of the flow burst region (750 m/s) and the resultant boundary motion speed determined from the linear regression (575±42 m/s) is the order of the maximum error velocity in the present analysis (150 m/s). Therefore the criterion for identifying the flow burst region (750 m/s) is justified.

In order to prove the presence of reconnection, we need to show that the plasma flow speed at the boundary is higher than the boundary motion speed. The velocities to the right of the dotted vertical line in Figure 4 represent mean flow speeds of the flow burst region together with their errors and standard deviations. The vertical dotted line is drawn at the start of the flow burst; the three data points before the flow burst onset will be explored in the discussion section. In the calculation of the mean velocity, we excluded the data with errors grater than 150 m/s. The shaded bar represents the boundary motion speed determined from Figure 3 (575±42 m/s). The mean flow speed in every scan after 2316 UT is significantly greater than the boundary motion speed. Hence it follows that in a frame moving with the separatrix, there exists a plasma flow crossing the separatrix. In other words, a reconnection process exists at the boundary.

We can estimate the reconnection electric field using the formula $E_{rec} = B(V - U)$, where V and U represent the components of the plasma velocity and the separatrix velocity, respectively, in the direction normal to the separatrix (positive equatorward), and $B \approx 47,000$ nT is the magnetic field strength in the flow burst region at 400 km altitude. Here we assume that the separatrix is elongated perpendicular to the line-of-sight direction of the radar. This assumption is reasonable, because the average poleward boundary of the auroral oval in this MLT sector is not L-shell-aligned but tilted in favor of this assumption [e.g., *Holzworth et al.*, 1975]. With $U = 580$ m/s and $V = 880$ m/s (total average throughout the flow burst period) determined from Figures 3 and 4, we obtain $E_{rec} = 14$ mV/m.

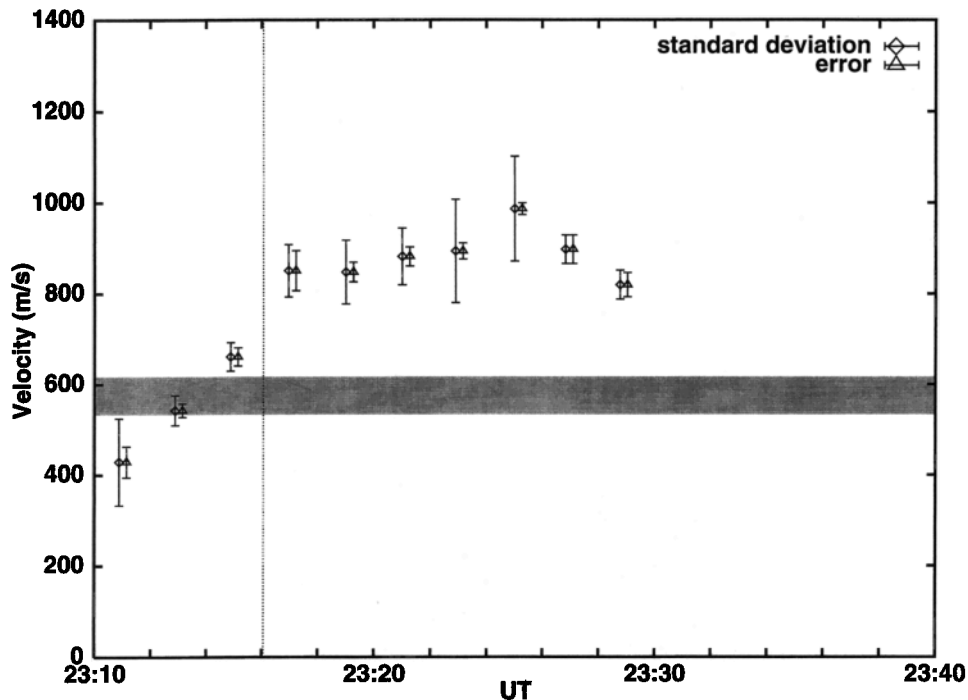If we can determine the azimuthal length of reconnection

Figure 4. (right of the dotted vertical line) The mean plasma flow speed of the flow burst region in each scan of the November 16 event, together with its standard deviation and error. The shaded bar shows the boundary motion speed determined from the linear regression in Figure 3. (left of the dotted vertical line) The mean plasma flow speed at the "virtual" boundary prior to the occurrence of the flow burst. The location of the virtual boundary was determined from the extrapolation of the linear regression in Figure 3.

region (L), we can also calculate the reconnection voltage along the X line using the formula $\Phi_{rec} = B(V - U)L$. With the present approach, we cannot determine the exact longitudinal scale of the reconnection region, because the line-of-sight velocity is not necessarily the total velocity and because the extent of the flow burst region may depend on the criterion we employ in identifying the flow burst region. Thus the azimuthal dimension of the flow burst region is a minimum estimate of the longitudinal scale of the reconnection region. Nevertheless, considering that the line-of-sight velocity is the dominant component of the velocity and that the criterion speed (750 m/s) is not an unreasonable value, our estimate is not so far from the actual value. During the main course of the flow burst, on average, the flow burst region was elongated from beam 7 to beam 11 at range 20, which corresponds to $L = 290$ km at 400 km altitude. With this value, the reconnection voltage is estimated to be 4.1 kV.

2.2. October 27, 1995, Event

The second event occurred on October 27, 1995, and its morphology was almost the same as the first example. Figure 5 shows the horizontal component (positive geomagnetic north) of ground-based magnetic disturbances observed at Thule (THL, near geomagnetic north pole), Dawson (DAW, auroral zone in the evening sector), Meanook (MEA, auroral zone in the evening sector), Ottawa (OTT, midlatitude in the evening sector), and Narssarssuaq (NAQ, premidnight auroral zone). See Table 1 for the locations of all these stations in geographic and geomagnetic coordinates. October 26 was a quiet day associated with a northward IMF for most of the day; the sum of Kp was 6. After ≈2140 UT on October 26, the near-Earth IMF (IMP 8 observation) was stable and northward with $B_z \geq$

5nT until it turned southward around 0030 UT on October 27. At 0037 UT on October 27, an eastward ionospheric electrojet started to grow in the evening sector (Dawson, Meanook, and Ottawa) as shown by the vertical dashed line on the left in Figure 5. At nearly the same time, a polar cap electrojet enhancement was also observed at Thule. These indicate that the growth phase of a substorm started at 0037 UT. After some variable magnetic activity, a small negative bay develops at Narssarssuaq at 0203 UT (the vertical dashed line on the right). This is the onset of the substorm expansion phase. Thus the substorm occurred after a long period of a quiet magnetosphere associated with a northward IMF. The time interval bounded by the two vertical dashed lines is the growth phase of the substorm. Bursts of flow similar to the previous example occurred from 0136 to 0158 UT as designated by the horizontal bar at the bottom panel of Figure 5 (Narssarssuaq magnetogram). These bursts occurred in the late growth phase just prior to the expansion phase onset.

Plate 3 shows a time sequence of Doppler velocities observed by the Goose Bay radar for each two-minute scan from 0130 to 0154 UT in the same format as Plate 1. The field of view covers the interval from 2200 to 0000 MLT. In Plate 3f (0140–0142), we can discern a localized enhanced bursty flow region whose Doppler velocity is >750 m/s equatorward (light-blue region) as indicated by a yellow arrow. In the subsequent scans, the bursty flow region migrates equatorward with time (Plates 3g–3k) and then it starts to degenerate at ≈ 0152 (Plate 3l, 0152–0154). The flow burst continued to migrate equatorwards and finally faded away at ≈ 0158 UT (not shown here). In this case, the flow burst signature disappeared before the expansion phase onset (0203 UT). We should bear in mind,
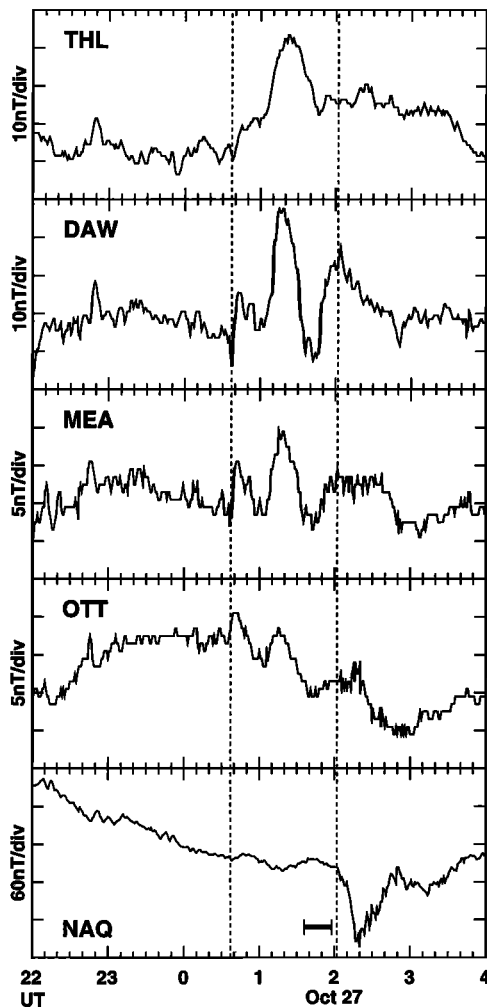
Figure 5. The horizontal component (positive geomagnetic north) of the geomagnetic field observed on October 27, 1995, at Thule (THL), Dawson (DAW), Meanook (MEA), Ottawa (OTT), and Narssarssuaq (NAQ) (see Table 1). The vertical dashed lines show the start of the substorm growth phase (0037 UT) and the onset of the expansion phase at Narssarssuaq (0203 UT). The bursty flow occurred during the time interval designated by the horizontal bar in the bottom Narssarssuaq magnetogram.

histograms of errors in the total magnitude and of errors in one component (north-south or east-west) of the calculated vectors in Figure 6 in order to quantify the accuracy of the vectors. The mode of the total magnitude error was 110 m/s, and its upper quartile (ninth decile) was 164 m/s (211 m/s). Similarly, the mode of the one-component error was 70 m/s, and its upper quartile (ninth decile) was 113 m/s (158 m/s). These show that the uncertainty of the vectors in Figure 6 is typically 100 m/s and mostly < 200 m/s. Vectors with magnitude < 100 m/s are replaced with solid circles in Figure 6.

The shaded areas in Figure 6 are high flow speed (> 750 m/s) regions (see Plate 3) associated with backscattered-power peaks (given below). These areas are located in the central part of the flow burst. Velocity vectors in the shaded regions are directed almost toward the Goose Bay radar site, which allows us to discuss the flow burst characteristics using exclusively Goose Bay data as in the previous event.

During the time interval of the bursty flow, DMSP F10 passed over the field of view of the Goose Bay radar flying poleward at altitudes of 760–780 km. Plate 4 shows energy versus time spectrograms of precipitating electrons (top panel) and ions (bottom panel) in the energy range from 30 eV to 30 keV in the same format as Plate 2. In this case, the transition from plasma sheet to polar cap is rather clear. At 0142:51 UT (MLAT=75.1°N, MLON=9.0°E, designated by a yellow wedge in Plate 4), the satellite observed an abrupt break off of plasma sheet electron precipitation; after that the electron spectra are very soft, showing a polar-rain-like signature. Ion precipitation also shows a flux drop off a little equatorward of the electron flux drop. Therefore we infer that the satellite's location at 0142:51 UT marks the open-closed boundary (separatrix).

The trajectory of DMSP F10 is shown in Plate 3g by an orange curve. The polar cap boundary is observed within this scan. The blue triangle on the trajectory shows the polar cap or open-closed (O/C) boundary observed at 0142:51 UT. From Plate 3g, we can discern that the bursty flow occurred near the separatrix; however, the light-blue high flow speed (> 750 m/s) region is somewhat fragmented and the spatial relationship between the separatrix and the center of the bursty flow region is not necessarily clear. In this event, we could use another parameter to identify the location of the separatrix. Plate 5 shows backscattered power that corresponds to Plate 3g. The orange curve shows the satellite trajectory and the blue triangle on the curve represents the polar cap boundary observation at 0142:51 UT. In Plate 5, we can see a power peak associated with the open-closed boundary, namely the small yellow and orange region to the right of the blue triangle on the DMSP track. *Walker et al.* [1987] provided a theoretical framework of backscattered power for an HF radar. They showed that the backscattered power falls off as the square of the range. The enhancements in power above the inverse square law curve could be attributable to either ionospheric focusing effects or production of strong irregularities. *Walker et al.* [1987] suggested that the focusing would only produce enhancements in power of a few decibels. Plate 5 shows that the power value at the peak is ~10 dB higher than the value of the surrounding regions. Therefore the power enhancement in Plate 5 indicates that there is a region with strong irregularity production. Such strong irregularity could be due to large electron density gradients, plasma velocity shears, or intense particle precipitation. *Baker et al.* [1990] noted that the dayside cusp was found to be a region of relatively high radar backscatter power compared to surrounding regions, indicating that 10-m scale ionospheric
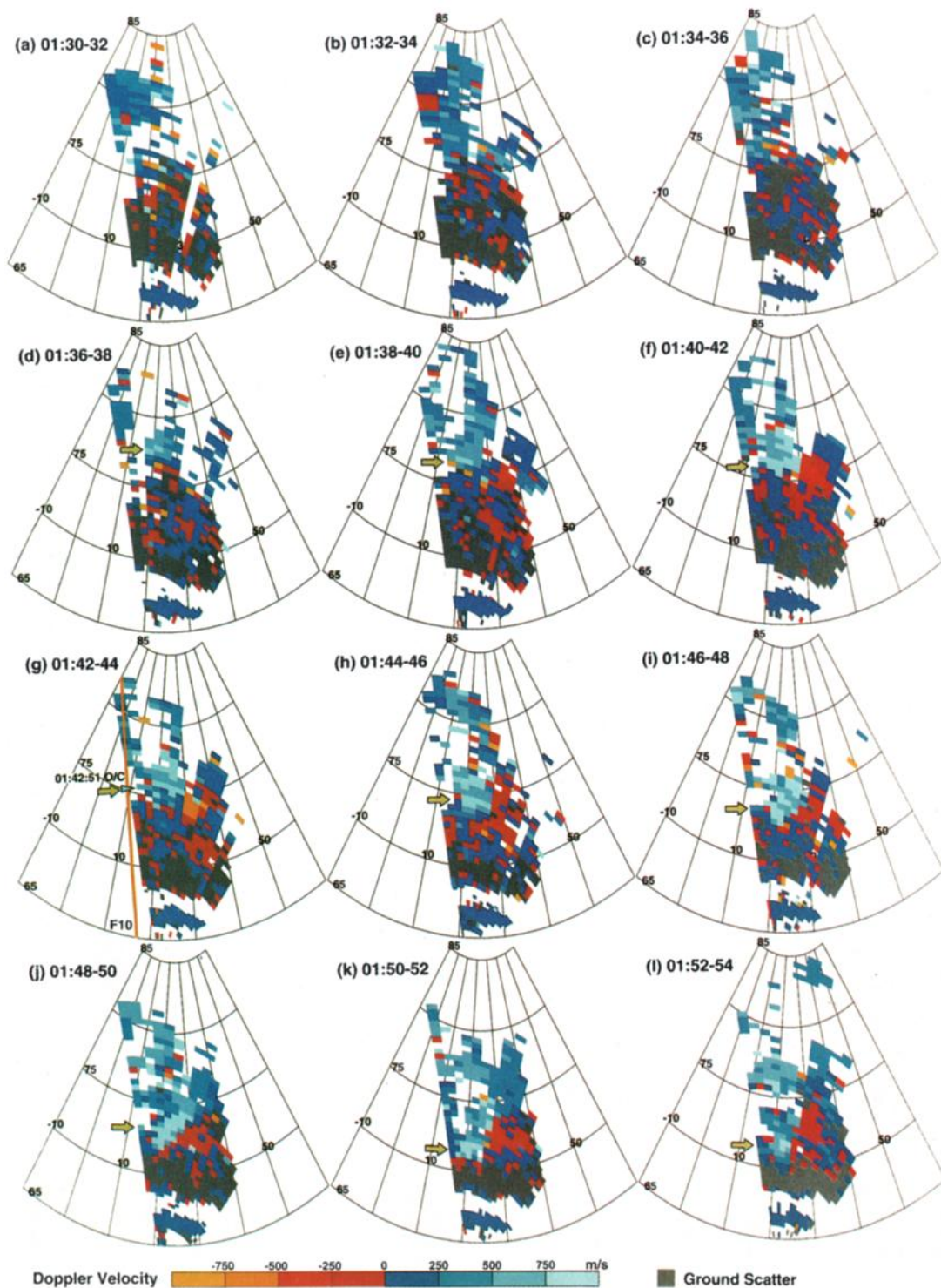
however, that the disappearance at 0158 UT occurred near the equatorward edge of F region echoes, and it is likely that the flow burst left the F region field of view of the radar after 0200 UT. Therefore we cannot know the whereabouts of the flow burst after 0200 UT even if it reappeared and migrated further equatorward. The flow burst can be backtracked to scan 0136–0138 (Plate 3d). Prior to that time there is no evidence of high flow speed regions (Plates 3a–3c). To summarize, an equatorward bursty flow region with velocities > 750 m/s emerged abruptly at ≈ 0136 (Plate 3d) and grew while migrating equatorward with time; it started to weaken at ≈ 0152 (Plate 3l) and finally died away at ≈ 0158 UT (not shown here).

Figure 6 shows two-dimensional velocity vector maps determined by the Goose Bay-Stokkseyri radar pair during the interval of major flow bursts (0140–0152 UT) in the same format as Figure 2. Figures 6a–6f correspond, respectively, to Plates 3f–3k. A median filter and a divergence-free relaxation technique are also used here. As in the previous event, we made

Plate 3. A time sequence of line-of-sight Doppler velocities observed by the Goose Bay radar during 0130–0154 UT on October 27, 1995, in the same format as Plate 1. The bursts of flow, designated by yellow arrows, emerged at ≈ 0136 UT (Plate 3d) and started to degenerate at ≈ 0152 UT (Plate 3l), and finally faded out at ≈ 0158 UT (not shown here). DMSP F10 passed over the field of view during this interval and observed the polar cap or open-closed boundary at 0142:51 UT (75.1°N, 9.0°E in AACGM coordinates). The trajectory of the satellite is shown in Plate 3g by an orange curve with the blue triangle marking the open-closed boundary.

irregularities were preferentially generated within the cusp. Since the same physical process (i.e., reconnection) is expected to occur on the nightside, the power hotspot in Plate 5 may be caused by strong irregularity associated with reconnection.

(Quantitative proof of reconnection will be given below.) Thus we can use the power peak as a tracer of the phenomenon and determine the separatrix motion less ambiguously. The power peak was identified from the start of the bursty flow (Plate 3d)
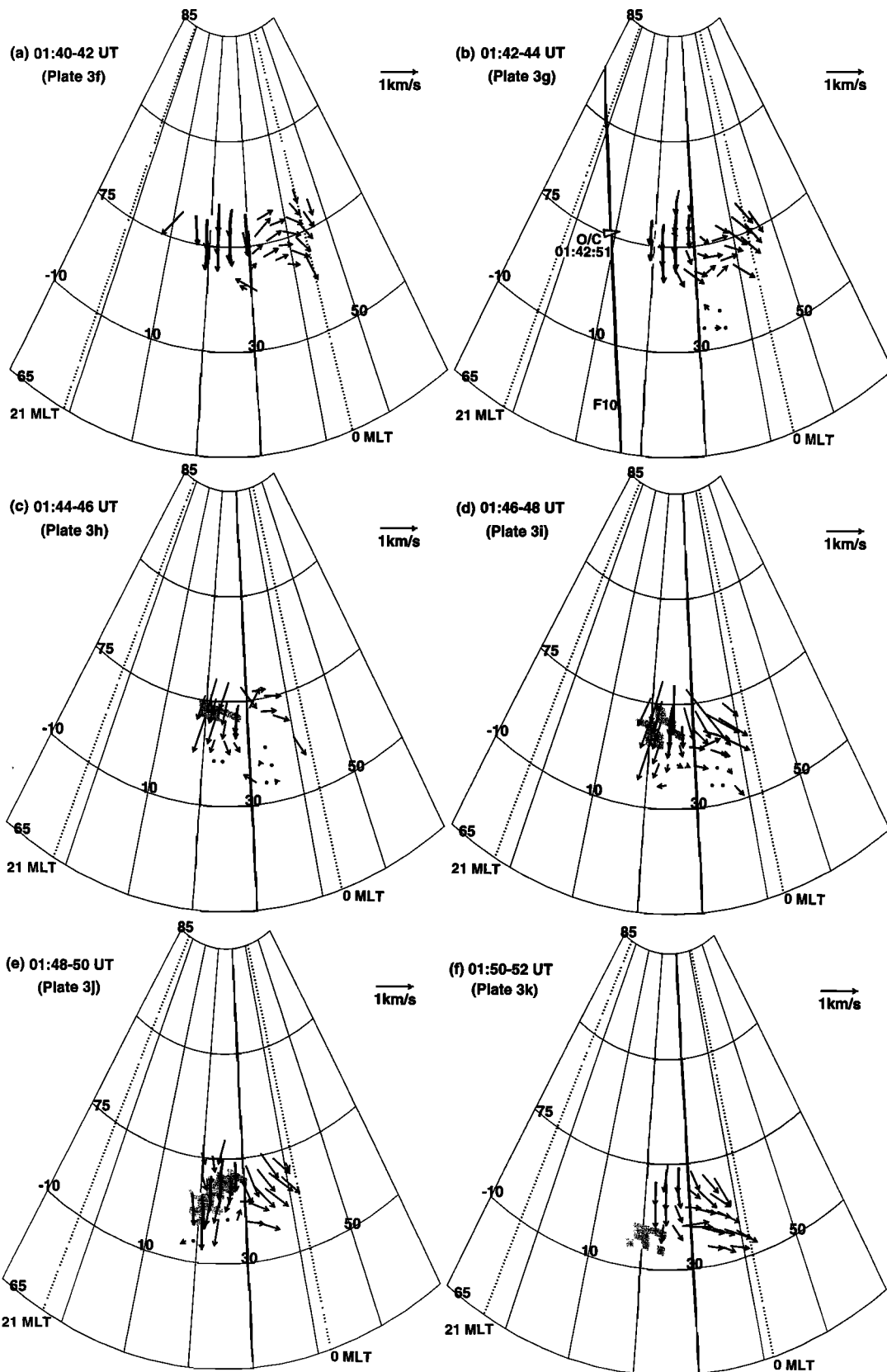
Figure 6. Two-dimensional velocity vectors during six scans between 0140 and 0152 UT on October 27, 1995, determined by combining the line-of-sight components from both Goose Bay and Stokkseyri data, in the same format as Figure 2. Figures 6a–6f correspond, respectively, to Plates 3f–3k. The gray shaded areas show the center of the flow burst region associated with >750 m/s velocities (Plate 3) and with a power peak. The solid curve in Figure 6b represents the trajectory of DMSP F10, and the solid triangle on the curve denotes the open-closed (O/C) boundary observation at 0142:51 UT.
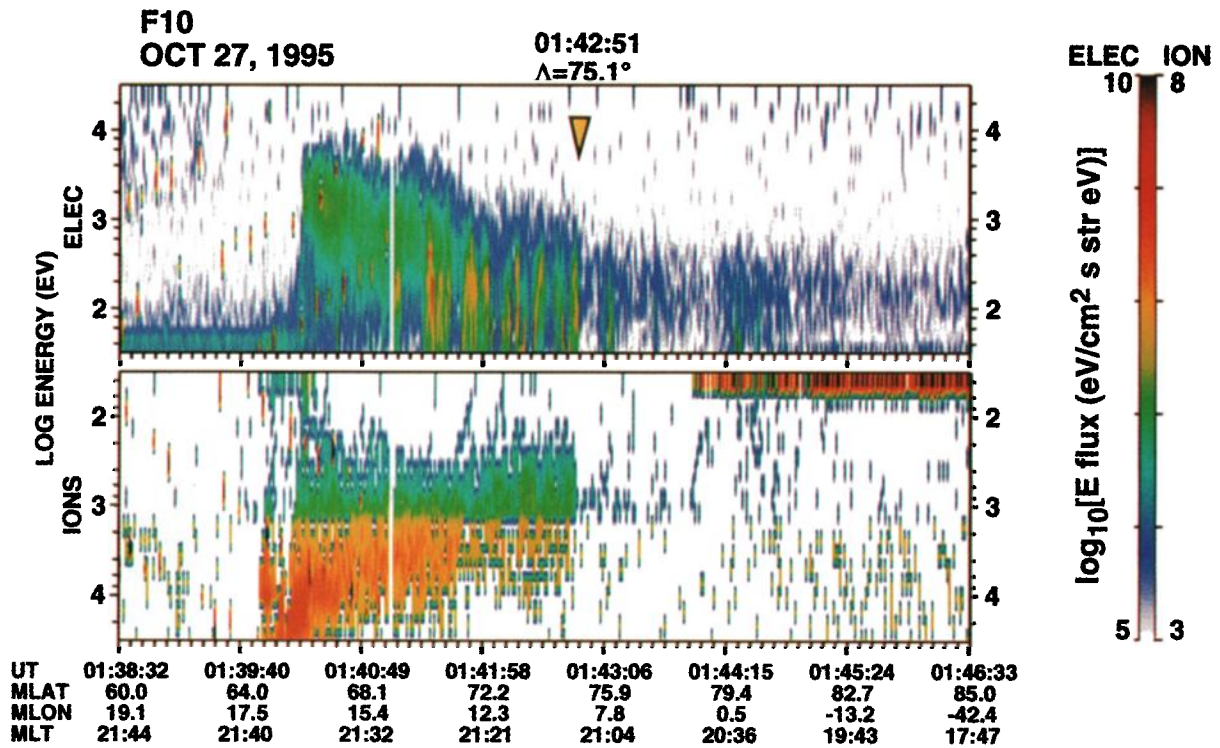
Plate 4. Energy versus time spectrograms of (top) precipitating electrons and (bottom) ions observed by the DMSP F10 satellite for the October 27, 1995, event, in the same format as Plate 2. The yellow wedge in the top designates the transition from plasma-sheet-like to polar-rain-like electron precipitation, which we infer is the open-closed boundary. The time and magnetic latitude of the open-closed boundary observation are shown at the top.
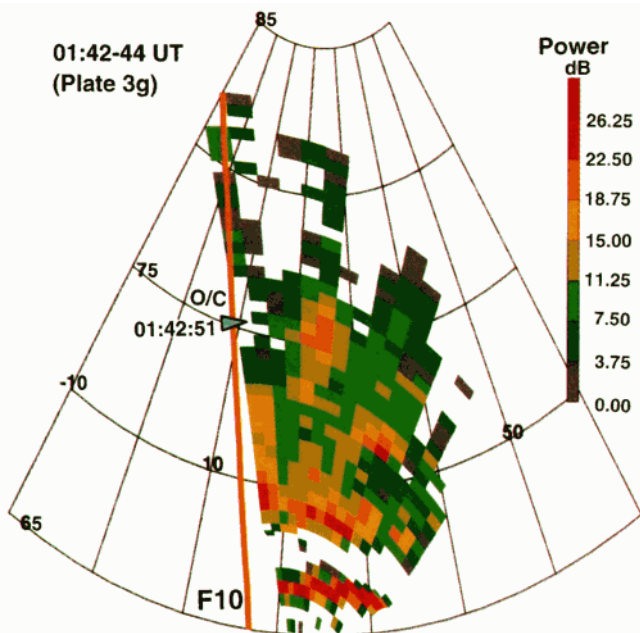

Plate 5. A two-dimensional map of backscattered power for the scan coinciding with the DMSP-10 open-closed boundary observation in the October 27 event. This scan corresponds to Plate 3g and Figure 6b. The orange curve shows satellite trajectory and the blue triangle designates the open-closed (O/C) boundary observation.

to the scan of Plate 3j (for the period of 0136–0150), but after that the power peak disappeared. The disappearance of the power peak is soon followed by the fading of the flow burst. This also justifies the use of the power peak as a tracer of the flow burst phenomenon associated with reconnection. (In passing, for the first example of November 16, 1995, we could not identify a clear power peak associated with the flow burst; overall, the backscattered power was generally high and showed an unstable pattern.)

The satellite trajectory is also plotted in Figure 6b together with the O/C boundary observation denoted by the solid triangle. Figure 6b corresponds to Plate 3g and Plate 5. We can conclude from Plate 3g, Plate 5, and Figure 6b that the bursty flow occurred at the polar cap boundary. Hence it is suggested that the equatorward migration of the bursty flow region corresponds to the equatorward motion of the polar cap boundary during the late substorm growth phase just prior to the expansion phase onset. With this assumption, we can determine the motion of the separatrix. Figure 7 shows the range (latitudinal) width of the "flow burst region" shown in Plate 3. Here we defined the flow burst region as a region of Doppler velocities > 750 m/s associated with a power peak (when identified). On average, the flow burst region was centered on beam 4. The oblique dotted line in Figure 7 is a linear regression line of the boundary motion. Since one range gate corresponds to 45 km, the speed of the boundary motion is estimated to be 669±23 m/s from the linear regression.
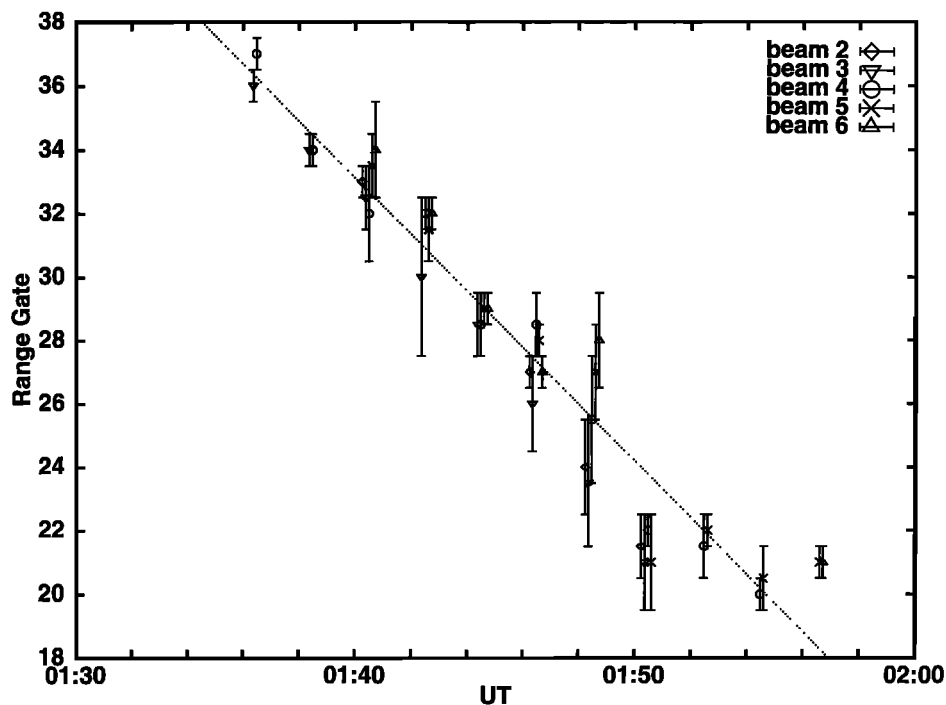
Figure 7. The range gate extent of the "flow burst region" on October 27, 1995, defined as the region of equatorward velocities greater than 750 m/s and associated with a power peak (when present) (Plates 3d–3l and two more scans onward not shown in Plate 3), in the same format as Figure 3. The oblique dotted line shows the linear regression fit. The boundary motion speed determined from the linear regression is 669±23 m/s.

As in the November 16 event, the next step is to show that the plasma speed is higher than the boundary motion speed. Averaged flow speeds of the flow burst region are shown in Figure 8 to the right of the vertical dotted line together with their errors and standard deviations. The vertical dotted line represents the start of the flow burst, and the three data points before the flow burst onset will be explored in the discussion section. In the statistics, we excluded the data with errors > 150 m/s. The shaded bar represents the boundary motion speed determined from Figure 7 (669±23 m/s). The mean flow speed in each scan is significantly greater than the boundary motion speed. Therefore we can conclude that the flow burst is a consequence of magnetic field reconnection.

Now we will estimate the reconnection electric field and voltage. Reconnection electric field is given by $E_{rec} = B(V - U)$; in this case, $B \approx 48000$ nT. With $U=670$ m/s and $V=890$ m/s (total average throughout the flow burst period) determined from Figures 7 and 8, and assuming that the separatrix is elongated perpendicular to the line-of-sight direction of the radar, we obtain $E_{rec}=11$ mV/m. Reconnection voltage is given by $\Phi_{rec} = B(V - U)L$. If we further assume that the average reconnection region is elongated from beam 2 to beam 6 at range 27, the azimuthal dimension of the reconnection region (L) is 380 km. Consequently, the reconnection voltage estimated is 4.0 kV, which is nearly the same value as determined in the previous November 16 event.

3. Discussion

3.1. Supplements to the Interpretation of the Flow Burst

3.1.1. The role of ionospheric conductivity. Although we interpreted the flow bursts presented in this paper as resulting

exclusively from magnetospheric processes, there may be an alternative interpretation of the data. There are several reports in the literature that suggested that the ionospheric conductivity modifies the electric field pattern and produces flow bursts [e.g., *Morelli et al.*, 1995; *Lewis et al.*, 1997]. *Morelli et al.* [1995] argued that a high Hall conductivity region creates an obstacle which diverts the background flow around it. Thus, to conserve the mass and momentum, the plasma accelerates around the obstacle. The direction of the flow burst is conditioned by the relationship between the enhanced conductivity and the pre-existing ionospheric flow. If the pre-existing flow is equatorward, an equatorward flow burst is produced to the west of the high conductivity region as described by Figure 11 of *Morelli et al.* [1995]. The flow pattern in our Figures 2 and 6 are similar to the cartoon in Figure 11 of *Morelli et al.* [1995]. Therefore an alternative interpretation may be possible: The equatorward flow bursts were guided by conductivity enhancements to the east of the flow bursts. However, we checked this possibility as follows, and concluded that the enhanced-conductivity-induced flow burst is unlikely.

For both events, the incoherent scatter radar at Sondre-stromfjord (the Sondrestrom IS radar) was in operation and we can make use of the data (by courtesy of R. A. Doe). The location of Sondrestromfjord is 67.0°N 309.1°E in geographic coordinates and 73.4°N 41.8°E in AACGM coordinates. During the November 16 event, the radar was performing elevation scans in the plane of the magnetic meridian. For this study, one scan of data from 2316 to 2319 UT was available, which corresponds to Plates 1d and 1e when the flow burst had just appeared. The radar measured the ionosphere 370 km east of the center of the flow burst. The E region (F region) electron density was about 0.6–4×10^{10} m^{-3} (1×10^{11} m^{-3}), showing
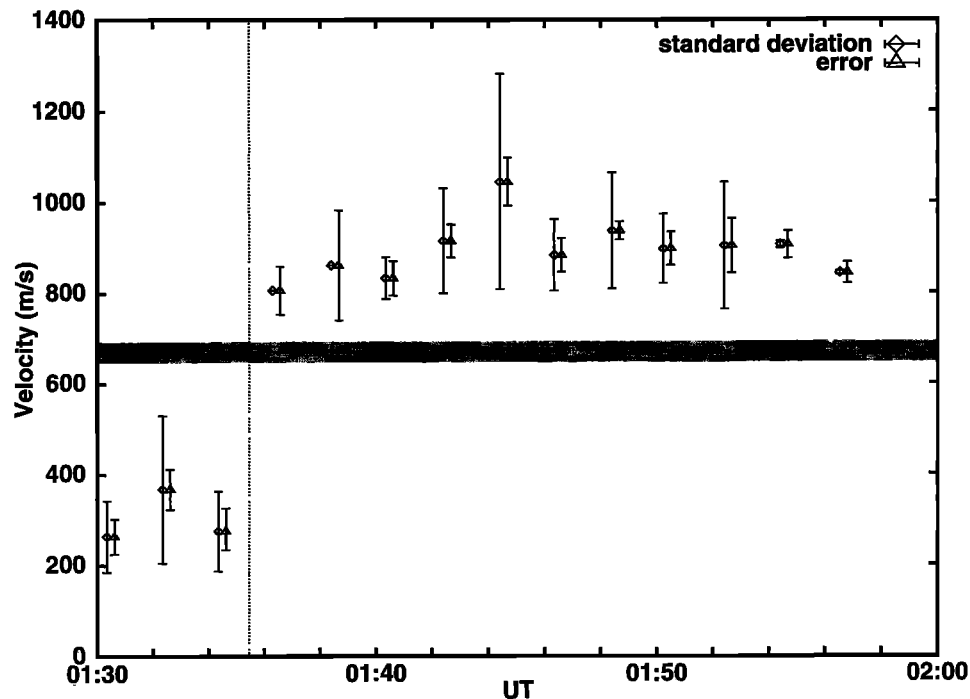
Figure 8. (right of the dotted vertical line) The mean plasma flow speed of the flow burst region in each scan of the October 27 event, together with its standard deviation and error. The shaded bar shows the boundary motion speed determined from the linear regression in Figure 7. (left of the dotted vertical line) The mean plasma flow speed at the "virtual" boundary prior to the occurrence of the flow burst. The location of the virtual boundary was determined from the extrapolation of the linear regression in Figure 7.

that the Hall conductivity was of the order of 1S. In addition, DMSP F12 passed 530 km east of the flow burst for 2324–2326 UT (Plate 1h). The energy time spectrograms in Plate 2 show that the precipitation to the east of the flow burst region is characterized by < 400 eV electrons. Electrons with such energies cannot ionize the ionosphere below 200 km [e.g., *Banks et al.*, 1974]. Thus we can conclude that there was no conductivity enhancement to the east of the flow burst.

For the October 27 event, the Sondrestrom IS radar was continuously looking up at a fixed position in the magnetic field direction. The distance between the flow burst and the radar observation region is 590 km at their closest approach. Throughout the time of our interest, the electron concentration in the E region (F region) was below 7×10^9 m^{-3} (about $3-4 \times 10^{10}$ m^{-3}). In this event, the Goose Bay radar observed a well-isolated backscattered power peak, which we suggest may be caused by similar processes (precipitation/flow shear/ density gradient) to those that produce the power peaks seen in dayside reconnection regions. If there is a strong precipitation region to the east of the flow burst, we expect that some signatures in the power would also appear to the east of the flow burst. However, no such signatures observed. All things considered, we infer that there was no conductivity enhancement also in this event.

3.1.2. Incompressible ionosphere. The entire ionospheric flow pattern is incompressible, i.e., divergence free. It follows that if plasma is driven from a particular location, much of the plasma in the surrounding ionosphere is also driven to satisfy the conservation of mass. In the October 27 event, the enhanced flow (>750 m/s) starts in a narrow region (Plates 3d and 3e) and grows in area at 0140 UT (Plate 3f). The growth may be interpreted as flows induced both poleward of and

equatorward of the reconnection region by the "incompressible ionosphere." Furthermore, an even more noteworthy feature in Plate 3 is that once the fast flow is established, the region of poleward flow emerges to the east of the flow burst and becomes more consistent as the velocity enhancement increases (Plates 3f–3j). This too could be the result of the return flow induced by the incompressible ionosphere. Such effects of incompressible ionosphere were described by *Southwood* [1987] but in the context of dayside reconnection signatures.

The effect of incompressible ionosphere appears to be observable also in the November 16 event. After the growth of the flow burst at 2318 UT (Plate 1e), a sunward and westward flow appears in the polar cap region to the northeast of the flow burst and enhances with time (Figures 2b–2d). This flow is also observed by DMSP F12 (Plate 2) as the high-speed cross-track ion drift just poleward of the open-closed boundary. Some portion of this flow could be attributable to the incompressible ionosphere. In the magnetosphere, a fast rarefaction wave is launched from the premidnight reconnection region into the polar cap and accelerates the plasma towards the reconnection region. In addition to the incompressible ionosphere, this fast mode wave in the magnetosphere would also contribute to the strong sunward and westward flow just poleward of the open-closed boundary.

3.1.3. Detached ions in the polar cap (November 16 event). As we noted previously, the ion observations in Plate 2 indicate a detached precipitation region poleward of the inferred open-closed boundary. Here we suggest a possible interpretation of these detached ions. Separatrix identification using precipitating particles often does not work on the dawnside and the duskside, because the so-called soft zone precipitation at high latitudes exhibits spectral characteristics intermediate between

mantle and cleft (closed boundary layer) signatures. This seems to occur preferably for geomagnetically quiet periods. *Lyons et al.* [1996] defined a region of soft-electron and magnetosheath-like ion precipitation (the soft-electron zone (SEZ)) lying between the plasma sheet and the region of polar rain on the morningside and the afternoonside to emphasize the potential connection to the solar wind of this region. Namely, they interpreted that the large portions of the SEZ are on open field lines. *Lyons et al.* [1996] demonstrated polar maps of particle precipitation for stable IMF intervals during the January 1992 GEM campaign period. Their map for a period of $B_z \gg |B_y|$ ($B_x = 7.6$ nT, $B_y = -1.9$ nT, and $B_z = 6.8$ nT) (their Figure 8) shows that the duskside SEZ extends up to 2100 MLT and the dawnside SEZ reaches 0100 MLT. We suspect that the detached ions observed poleward of the inferred open-closed boundary are such magnetosheath-like particles that Lyons et al. called SEZ. Unfortunately we have no IMF data from 2043 to 2259 UT and cannot know the IMF conditions just prior to the southward turning of the IMF. However, the 1.5-hour-averaged near-Earth IMF prior to 2043 UT was $B_x = 5.2$ nT, $B_y = -1.5$ nT, and $B_z = 1.9$ nT (IMP 8 observations) and is not inconsistent with the IMF conditions in the case study of Lyons et al. Therefore we infer that during the northward-IMF period before the growth phase, particles of magnetosheath origin were encircling the polar cap boundary up to the nightside and the detached ions observed by DMSP F12 (Plate 2) are remnant of these particles. In fact, in the preceding DMSP F12 pass over the northern hemisphere at $\approx$2146 UT, similar soft ions were also observed near the polar cap boundary. In addition, in that DMSP pass, isolated polar cap arc precipitation characteristic of northward IMF B_z periods was clearly observed. The detached ion precipitation in Plate 2 starts at or a little poleward of the inferred open-closed boundary. This is reasonable if the ions are of solar wind origin.

3.2. Comparison With Previous Reconnection Measurements

We have determined the reconnection electric field and voltage for nightside reconnection just prior to the substorm expansion phase onset. First of all, we will compare our present results with the two previous studies on this subject, *de la Beaujardière et al.* [1991] and *Blanchard et al.* [1996].

The reconnection electric field at 400 km altitude determined in this study is 14 mV/m (2030 MLT sector) for one case and 11 mV/m (2300 MLT sector) for the other case. *Blanchard et al.* [1996] investigated the local time dependence of the reconnection electric field and showed that on average the reconnection electric field is highest in the 4-hour local time sector between 2130 and 0130 MLT with average values ranging from 12 to 16 mV/m. *De la Beaujardière et al.* [1991] found that the reconnection electric field during times of local polar cap expansion (observations mostly during the substorm recovery phase) was <15 mV/m. Therefore our present results are consistent with previous results.

The reconnection voltage integrated along the X line determined in this paper is about 4 kV for both events. The MLT profile of average reconnection rate determined by *Blanchard et al.* [1996] showed that the potential drop across the 4-h region of 2130–0130 MLT was 29 kV. Therefore the reconnection observed in this study accounts for only one seventh of the average potential drop of the 4-h main reconnection region. It is of interest to determine whether the 4 kV scale reconnection is an element of several distant tail reconnection

processes with the total potential drop being the sum of the several processes. This is a subject for future research.

3.3. Activation of the Distant Tail Neutral Line in Response to the Southward Turning of the IMF

The substorms investigated here occurred after a long period of magnetospheric inactivity associated with a northward IMF. Therefore the nightside reconnection revealed in this paper is taken to be a magnetospheric response to the southward turning of the IMF, namely to dayside reconnection. Both flow bursts started ~1 hour after the growth phase onset. *Blanchard et al.* [1996] showed that the nightside reconnection electric field is correlated with IMF B_z with a 70-min lag, so our present observations are consistent with this previous work. The time lag is suggested to be the timescale on which the distant tail neutral line is activated as a consequence of dayside reconnection. We will discuss this timescale here.

After reconnection on the dayside magnetopause commences, solar wind plasma enters the magnetosphere and fills the tail lobes. For the moment let us assume that the solar wind plasma expands into vacuum tail lobes. MHD theory tells us that only a slow rarefaction wave allows expansion into the vacuum. Therefore the formation of the plasma mantle or high-latitude boundary layer can be modeled by a slow expansion fan [*Siscoe and Sanchez*, 1987]. In the real magnetosphere, the lobes are not a vacuum; hence a contact discontinuity will precede the slow expansion into the tail lobes. The discontinuity separates the plasmas of solar wind origin from the plasmas of Earth origin. The slow rarefaction waves from the northern and southern tail lobes will converge at some finite distance downstream in the equatorial magnetotail. *Coroniti* [1985] suggested in his conceptual substorm model that since open field lines can first come into contact near the wave closure region, the distant tail neutral line should be located there. The morphology determined here agrees with his model.

From the approach in this paper, we cannot determine the exact start time of the reconnection rate enhancement, because reconnection may have been started prior to the start of the flow burst. However, in the second example of October 27, 1995, the flow burst and the backscattered power enhancement started at the same time. As we discussed previously, the power enhancement may be due to strong field-aligned irregularities associated with the reconnection process. Therefore it is suggested that the reconnection rate enhancement started at nearly the same time as the flow burst start for the October 27 event. As for the other event on November 16, 1995, although we could not trace power peaks, we can show that if the boundary motion speed is constant, the start of the reconnection could only precede by one scan (two minutes) the start of the flow burst (see the discussion in section 3.4.2 concerning the left-hand side of Figure 4). Hence we infer that for the November 16 event, the start time of the reconnection rate enhancement is not significantly separated from the flow burst start time. For a qualitative discussion, it is sufficient to assume that the reconnection rate enhancement and the flow burst started at the same time.

For the November 16 event, the growth phase started at 2219 UT and subsequently the flow burst started at 2316; the time span between the two phenomena is 57 min. For the October 27 event, the start of the growth phase was 0037 UT and that of the flow burst was 0136 UT; the time span between the two phenomena is 59 min. These time lags are typical times

for the ionospheric plasma to move from the dayside cusp to the nightside polar cap boundary or equivalently for the mantle plasma to proceed from the dayside magnetopause to the distant tail neutral line. From the perspective of MHD waves, the time lag is the timescale on which slow rarefaction waves from the northern and southern lobes converge somewhere downstream in the equatorial magnetotail.

We can estimate the location of the distant tail neutral line from the time lag between the onsets of the growth phase and the flow burst. *Slavin et al.* [1985] determined X profiles of plasma parameters between $X = -50\ R_E$ and $X = -230\ R_E$ both for lobe and plasma sheet plasmas. Their results showed that average tailward flow speed in the lobes earthward of $X = -180\ R_E$ is about 150–200 km/s, which is about half of the typical solar wind speed. The average solar wind speed in the two events was 350 km/s for the November 16 case and 360 km/s for the October 27 case. If we assume for simplicity that the dayside eroded magnetic flux was conveyed from a dayside magnetopause located at $X = 10\ R_E$ to the distant tail at half the speed of the solar wind, namely, 175 km/s for the November 16 case and 180 km/s for the October 27 case, it follows that the distant tail neutral line occurs at $X = -84\ R_E$ and $X = -90\ R_E$, respectively. These estimates are reasonable when compared with a picture determined from in situ observations by ISEE 3 and Geotail spacecrafts, specifically for southward IMF periods. *Slavin et al.* [1985] reported that an X profile of plasma sheet parameters showed a sudden decrease in B_z and a super-Alfvénic flow onset near $X = -100\ R_E$, suggesting the presence of the distant tail neutral line at that location. This tendency becomes clearer for geomagnetically active times. *Slavin et al.* [1987] reported that for disturbed conditions ($|AL| > 100$ nT), magnetic fields are northward and the plasma flow is earthward inside $|X| = 90\ R_E$, but beyond that the fields are predominantly southward and the flow is tailward. *Nishida et al.* [1995] suggested that at least 75% of open field line reconnection occurs inside $|X| = 150\ R_E$ and at least 39% occurs inside $|X| = 95\ R_E$. Thus, at least for southward IMF, the distant tail neutral line is expected to occur near $|X| = 100\ R_E$, and our estimates are consistent with this.

3.4. Precursors to Substorm Onset

So far we have explored the flow burst phenomenon separately from substorms, with an emphasis on proving that it is associated with reconnection. However, the morphology of the flow burst is very important in that it occurs just prior to the substorm expansion phase onset. Here we will discuss it from the point of view of substorms.

3.4.1. Relationship between distant tail reconnection and the substorm onset.
It is believed that the distant tail neutral line always exits. Therefore, although the flow burst associated with the reconnection is observed just prior to the expansion phase onset, it would be hasty to conclude that distant tail reconnection triggers the substorm onset. For both events, the flow burst disappeared around the onset of the substorm. One may imagine a link between the reconnection and the substorm onset from this morphology, but the coincidence would be mainly due to the deceleration of the equatorward boundary motion by the enhanced reconnection rate on the nightside (including near-Earth reconnection) and by the magnetotail reconfiguration from tail-like to dipolar field after the substorm onset. In addition, in the November 16 case, the start of the negative bay was in the Scandinavian meridian (see Figure 1) and was well east of the flow burst meridian. Thus there is

not much evidence to conclude that the distant tail reconnection and the substorm onset are physically linked. The physical link between the two would be weak, and we may say in general that the deep tail reconnection is not a direct trigger of the substorm onset. It should be noted, however, that as we discuss below, the magnetotail configuration starts to be tail-like nonlinearly when the distant tail reconnection rate starts to increase. Hence it could be that the enhancement of the distant tail reconnection is indirectly coupled with the substorm onset via the nonlinear stretching of the magnetotail magnetic field. In this sense, there may be a weak tentative link between the distant tail reconnection and the substorm triggering, at least in the two events analyzed in this paper.

3.4.2. Rapid change of magnetotail configuration.
The ionospheric projection of the separatrix gives information on the magnetospheric configuration. In this paper, we have determined the separatrix motion just prior to substorm onsets. Here we will discuss the time development of magnetotail configuration inferred from the separatrix motion at the end of the growth phase.

While the plasma flow speed due to the reconnection electric field $(V - U)$ is 300 m/s for the November 16 event and 220 m/s for the October 27 event, the separatrix motion speed (U) is 580 and 670 m/s, respectively, for the two cases. Thus most of the flow burst is contributed by the boundary motion of several hundred meters per second. One may doubt whether the polar cap boundary can move at such high speeds. For example, if we backtrack the boundary with the same constant speed, we find that there is almost no polar cap at the start of the growth phase. We note, however, that the high-speed boundary motion is supported by previous observations. At present, the most reliable way to determine the location of the separatrix on the nightside from the ground observation is to use latitudinal profiles of 630-nm auroral emission [*Blanchard et al.*, 1995, 1997]. *Samson et al.* [1992] demonstrated for a well-isolated substorm on December 7, 1989, that the poleward boundary of 630-nm emission moved equatorward gradually with an average speed of several tens meters per second from the beginning of the growth phase up to ~5 min before the expansion phase onset. For the last 5 min of the growth phase prior to the expansion phase onset, the equatorward motion of the emission boundary increased steeply to a speed of several hundred meters per second. These results suggest that the polar cap boundary on the nightside moved much faster (several hundred meters per second) for the 5 min prior to the expansion phase onset than for the preceding early and middle growth phases. Although the timescale (several minutes) is somewhat shorter than the lifetime of the flow burst in this study, we infer that this auroral morphology is another view of the same phenomenon examined in this study.

When did the rapid boundary motion actually start in the two cases studied here? This question may be answered by determining the motion of the boundary prior to the appearance of the flow burst. The data in Figures 4 and 8 to the left of the vertical dotted line show the plasma flow speed at the "virtual" boundary prior to the appearance of the flow burst. Three data points in Figure 4 and three data points in Figure 8 correspond, respectively, to Plates 1a–1c and Plates 3a–3c. Here we calculated the mean value of the plasma velocity at the "expected" boundary location determined from the extrapolation of the linear regression in Figures 3 and 7, with an assumption of constant boundary motion speed throughout the events. In the case of the October 27 event (Figure 8), the

plasma flow speed at the (virtual) boundary prior to the flow burst onset is much lower than the (assumed) boundary motion speed. In the case of the November 16 event (Figure 4), the relative speed of the plasma is still positive or zero for the two scans before the flow burst start but it becomes negative for the third scan prior to the flow burst onset. Negative relative velocity of the plasma means that an equatorward moving separatrix on the nightside overtakes the equatorward moving plasma and the reconnection rate at the X line is negative. Within the accepted framework of reconnection this cannot be possible. Therefore we can conclude that the boundary speed prior to the start of the flow bursts must have been less than the boundary speeds derived from our regression analysis. The fast equatorward migration only started at 0136 UT for the October 27 case and at 2313 UT for the November 16 case, at nearly the same time as the flow burst onset.

Is the fast-moving boundary at the end of the growth phase a feature at all local times? The ionospheric projection of the separatrix is often modeled as a circle for simplicity. The polar cap expands equatorward during the growth phase due to the enhanced dayside reconnection rate. Let us assume for a moment that the expansion of the polar cap is independent of local time, namely, open flux added at the dayside cusp is uniformly redistributed over all local times to form a circular polar cap. If the dayside reconnection rate is constant, then the incremental change of the polar cap radius should diminish with time (since the area of the circular polar cap is proportional to the radius squared), which is the opposite of the observation. In reality, the solar wind parameters are not constant, and consequently the dayside reconnection rate would not be constant. Although we do not know exactly how the dayside reconnection rate depends on solar wind parameters, as an initial approximation we would expect the southward component of the IMF to contribute most to the dayside reconnection rate. The rapidly expanding polar cap at the end of the growth phase would require a steeply increasing southward IMF for the flow burst period. However, such a signature was not observed for both events: In the October 27 event, the IMF B_z that corresponds to the flow burst period (combined Wind and IMP 8 observations) remained constant with $B_z \approx -3.8$ nT for the first half and then decreased gradually in magnitude to -2.0 nT; in the November 16 event, the IMF B_z (IMP 8 observations) was nearly constant with a value of -5.0 nT (although there were some data dropouts). In addition, if we assume for simplicity that the center of the polar cap is fixed, a circular polar cap expansion with a velocity of 500 m/s will require a dayside reconnection of voltage of 190 kV (380 kV) when the polar cap radius is 10° (20°). Such a high reconnection voltage seems impossible for the observed IMF B_z; the dayside reconnection voltage is typically several tens of kilovolts [e.g., *Baker et al.*, 1997]. Thus the observational facts suggest that the circular polar cap model, i.e., a uniformly expanding polar cap, is no longer valid for the fast-moving boundary at the end of the growth phase. Instead, considering the proportionality of the polar cap area to the total amount of open magnetic flux, we should interpret that the fast-moving boundary feature is confined to the nightside.

Why does the polar cap expand nonuniformly? There are at least two factors that determine the shape of the separatrix: one is the magnetic flux budget through the separatrix by the reconnection processes, and the other is the magnetic field configuration itself. The fast-moving boundary at the end of the growth phase on the nightside would be attributable to the latter factor. The change of magnetospheric configuration re-

ally means the change of electric current distribution. The most plausible cause of the configuration change would be a more rapid intensification and/or earthward movement of the cross-tail current for the last stage of the growth phase. It is well known that during the growth phase, magnetic fields at geosynchronous altitude are distorted progressively to a more tail-like configuration until the expansion phase onset [e.g., *Sauvaud and Winckler*, 1980]. However, at geosynchronous altitude there seems to be no abrupt configuration change 10–20 min prior to the expansion phase onset as envisaged in this study.

Using AMPTE/CCE data in the near-Earth magnetotail ($|X| = 6-9$ R_E), *Ohtani et al.* [1992] have found that an "explosive growth phase" characterized by a sudden enhancement of growth phase perturbation (reduction of B_z) precedes the full onset of substorms. However, the timescale of their explosive growth phase is normally less than one minute and is much shorter than that (10–20 min) of the flow burst phenomenon studied in this paper. We infer that the explosive growth phase is a phenomenon associated with the expansion phase onset and essentially different from the global magnetotail configuration change in the late growth phase delineated in this study.

It is certain that the magnetotail configuration change happens nonlinearly at the end of growth phase, although we do not know the details of the process from the present study. However, we have shown that the nonlinear growth starts ~1 hour after the southward turning of the IMF and this time span corresponds to the timescale on which slow expansion fans from the dayside cusps fill the magnetotail lobes. We think this is important for future modeling of substorms.

4. Conclusions

1. Using simultaneous observations of Goose Bay-Stokkseyri dual HF radars and DMSP satellites, we have found ionospheric signatures of distant tail reconnection that lasts for 10–20 min just prior to substorm onsets. Our conclusions are based on flow bursts on the nightside during two isolated substorms (one on November 16, 1995, and the other on October 27, 1995) that followed a long period of magnetospheric inactivity associated with a northward IMF. For the November 16 event, the reconnection electric field at 400 km altitude was 14 mV/m and its longitudinal scale was 290 km, which is equivalent to a reconnection voltage of 4.1 kV. For the October 27 event, these values were 11 mV/m (reconnection electric field), 380 km (longitudinal scale), and 4.0 kV (reconnection voltage).

2. In addition to the reconnection signatures, we have discussed the implications of the flow bursts on substorm dynamics during the final stage of the substorm growth phase. The morphology suggests that a sudden enhancement of distant tail reconnection starts about 60 minutes after the growth phase onset (10–20 min prior to the expansion phase onset), and at the same time the nightside separatrix starts to move equatorward with a speed of several hundred meters per second, much faster than the preceding early and middle growth phases. The 1-hour time lag between the onsets of the growth phase and the distant-tail reconnection enhancement is consistent with the timescale on which slow expansion fans emanating from the dayside cusps fills the magnetosphere. This suggests that activation of the distant tail neutral line occurs as a result of the closure of slow rarefaction waves from the northern and southern tail lobes. The fast-moving separatrix on the nightside implies a rapid change of magnetotail configuration resulting from nonlinear enhancement and/or earthward movement of

the cross-tail current for the last 10–20 min of the growth phase prior to the expansion phase onset.

References

Baker, K. B., R. A. Greenwald, J. M. Ruohoniemi, J. R. Dudeney, M. Pinnock, P. T. Newell, M. E. Greenspan, and C.-I. Meng, Simultaneous HF-radar and DMSP observations of the cusp, *Geophys. Res. Lett., 17,* 1869–1872, 1990.

Baker, K. B., J. R. Dudeney, R. A. Greenwald, M. Pinnock, P. T. Newell, A. S. Rodger, N. Mattin, and C.-I. Meng, HF radar signatures of the cusp and low-latitude boundary layer, *J. Geophys. Res., 100,* 7671–7695, 1995.

Baker, K. B., A. S. Rodger, and G. Lu, HF-radar observations of the dayside magnetic merging rate: A Geospace Environment Modeling boundary layer campaign study, *J. Geophys. Res., 102,* 9603–9617, 1997.

Banks, P. M., C. R. Chappell, and A. F. Nagy, A new model for the interaction of auroral electrons with the atmosphere: Spectral degradation, backscatter, optical emission, and ionization, *J. Geophys. Res., 79,* 1459–1470, 1974.

Bhavnani, K. H., and C. A. Hein, An improved algorithm for computing altitude dependent corrected geomagnetic coordinates, *Phillips Lab. Tech. Rep. PL-TR-94-2310,* Phillips Lab., Hanscom Air Force Base, Mass., 1994.

Blanchard, G. T., L. R. Lyons, J. C. Samson, and F. J. Rich, Locating the polar cap boundary from observations of 6300 Å auroral emission, *J. Geophys. Res., 100,* 7855–7862, 1995.

Blanchard, G. T., L. R. Lyons, O. de la Beaujardière, R. A. Doe, and M. Mendillo, Measurement of the magnetotail reconnection rate, *J. Geophys. Res., 101,* 15,265–15,276, 1996.

Blanchard, G. T., L. R. Lyons, and J. C. Samson, Accuracy of using 6300 Å auroral emission to identify the magnetic separatrix on the nightside of Earth, *J. Geophys. Res., 102,* 9697–9703, 1997.

Coroniti, F. V., Explosive tail reconnection: The growth and expansion phases of magnetospheric substorms, *J. Geophys. Res., 90,* 7427–7447, 1985.

Cowley, S. W. H., and M. Lockwood, Excitation and decay of solar wind-driven flows in the magnetosphere-ionosphere system, *Ann. Geophys., 10,* 103–115, 1992.

de la Beaujardière, O., D. S. Evans, Y. Kamide, and R. P. Lepping, Response of auroral oval precipitation and magnetospheric convection to changes in the interplanetary magnetic field, *Ann. Geophys. A, 5,* 519–526, 1987.

de la Beaujardière, O., L. R. Lyons, and E. Friis-Christensen, Sondrestrom radar measurements of the reconnection electric field, *J. Geophys. Res., 96,* 13,907–13,912, 1991.

Greenspan, M. E., P. B. Anderson, and J. M. Pelagatti, Characteristics of the thermal plasma monitor (SSIES) for the Defense Meteorological Satellite Program (DMSP) spacecraft F8 through F10, *Tech. Rep. AFGL-TR-86-0227,* Hanscom Air Force Base, Mass., 1986.

Greenwald, R. A., et al., DARN/SuperDARN: A global view of the dynamics of high-latitude convection, *Space Sci. Rev., 71,* 761–796, 1995.

Hardy, D. A., L. K. Schmidtt, M. S. Gussenhoven, F. J. Marshall, H. C. Yeh, T. L. Shumaker, A. Hube, and J. Pantazis, Precipitating electron and ion detectors (SSJ/4) for the block 5D/flights 6-10 DMSP satellites: Calibration and data presentation, *Tech. Rep. AFGL-TR-84-0317,* Hanscom, Air Force Base, Mass., 1984.

Heelis, R. A., The effects of interplanetary magnetic field orientation

on dayside high-latitude convection, *J. Geophys. Res., 89,* 2873–2880, 1984.

Holzworth, R. H., and C.-I. Meng, Mathematical representation of the auroral oval, *Geophys. Res. Lett., 1,* 377–380, 1975.

Lewis, R. V., M. P. Freeman, A. S. Rodger, G. D. Reeves, and D. K. Milling, The electric field response to the growth phase and expansion phase onset of a small isolated substorm, *Ann. Geophys., 15,* 289–299, 1997.

Lockwood, M., S. W. H. Cowley, C. R. Clauer, H. Todd, S. R. Crothers, and D. M. Willis, Ion flows and heating at a contracting polar-cap boundary: GISMOS observations indicating viscous-like interaction on the flanks of the magnetotail, *Adv. Space Sci., 9(5),* 39–44, 1989.

Lyons, L. R., G. Lu, O. de la Beaujardière, and F. J. Rich, Synoptic maps of polar caps for stable interplanetary magnetic field intervals during January 1992 geospace environment modeling campaign, *J. Geophys. Res., 101,* 27,283–27,298, 1996.

Morelli, J. P., et al., Radar observations of auroral zone flows during a multiple-onset substorm, *Ann. Geophys., 13,* 1144–1163, 1995.

Nishida, A., T. Mukai, T. Yamamoto, Y. Saito, and S. Kokubun, GEOTAIL observations on the reconnection process in the distant tail in geomagnetically active times, *Geophys. Res. Lett., 22,* 2453–2456, 1995.

Ohtani, S., K. Takahashi, L. J. Zanetti, T. A. Potemra, R. W. McEntire, and T. Iijima, Initial signatures of magnetic field and energetic particle fluxes at tail reconfiguration: Explosive growth phase, *J. Geophys. Res., 97,* 19,311–19,324, 1992.

Reiff, P. H., R. W. Spiro, and T. W. Hill, Dependence of polar cap potential drop on interplanetary parameters, *J. Geophys. Res., 86,* 7639–7648, 1981.

Samson, J. C., L. R. Lyons, P. T. Newell, F. Creutzberg, and B. Xu, Proton aurora and substorm intensifications, *Geophys. Res. Lett., 19,* 2167–2170, 1992.

Sauvaud, J.-A., and J. R. Winckler, Dynamics of plasma, energetic particles, and fields near synchronous orbit in the nighttime sector during magnetospheric substorms, *J. Geophys. Res., 85,* 2043–2056, 1980.

Siscoe, G. L., and E. R. Sanchez, An MHD model for the complete open magnetotail boundary, *J. Geophys. Res., 92,* 7405–7412, 1987.

Slavin, J. A., E. J. Smith, D. G. Sibeck, D. N. Baker, R. D. Zwickl, and S.-I. Akasofu, An ISEE 3 study of average and substorm conditions in the distant magnetotail, *J. Geophys. Res., 90,* 10,875–10,895, 1985.

Slavin, J. A., P. W. Daly, E. J. Smith, T. R. Sanderson, K.-P. Wenzel, R. P. Lepping, and H. W. Kroehl, Magnetic configuration of the distant plasma sheet: ISEE 3 observations, in *Magnetotail Physics,* edited by A.T.Y. Lui, pp. 59–63, Johns Hopkins Univ., Laurel, Md., 1987.

Southwood, D. J., The ionospheric signature of flux transfer events, *J. Geophys. Res., 92,* 3207–3213, 1987.

Vasyliunas, M. V., Steady state aspects of magnetic field line merging, in *Magnetic Reconnection in Space and Laboratory Plasmas, Geophys. Monogr. Ser.,* vol. edited by E. W. Hones Jr., pp. 25–31, AGU, Washington, D. C., 1984.

Walker, A. D. M., R. A. Greenwald, and K. B. Baker, Determination of the fluctuation level of ionospheric irregularities from radar backscatter measurements, *Radio Sci., 22,* 689–705, 1987.

R. A. Greenwald, Applied Physics Laboratory, Johns Hopkins University, Johns Hopkins Road, Laurel, MD 20723-6099. (e-mail: ray_greenwald@jhuapl.edu)

M. R. Hairston, William B. Hanson Center for Space Sciences, University of Texas at Dallas, P.O. Box 830688 F022, Richardson, TX 75083-0688. (e-mail: hairston@utdallas.edu)

M. Pinnock and A. S. Rodger, British Antarctic Survey, Natural Environment Research Council, High Cross, Madingley Road, Cambridge, England, CB3 0ET U.K. (e-mail: mpi@pcmail.nerc-bas.ac.uk; asro@pcmail.nerc-bas.ac.uk)

N. Sato, M. Watanabe, H. Yamagishi, and A. S. Yukimatu, National Institute of Polar Research, 1-9-10 Kaga, Itabashi-ku, Tokyo 173-8515, Japan. (e-mail: nsato@nipr.ac.jp; maskaz@hp9000.nipr.ac.jp; yamagisi@nipr.ac.jp; sessai@nipr.ac.jp)

J.-P. Villain, Laboratoire de Physique et Chimie de l'Environnement, Centre National de la Recherche Scientifique, 3A Avenue de la Recherche Scientifique, 45071 Orléans, Cedex 2, France. (e-mail: jvillain@cnrs-orleans.fr)